in oligomer areas in Braak stage 0, III, and V brains, indicating that the oligomers in Braak stage I brains are smaller than those in Braak stage III or V brains. Indeed, in one Braak stage I case that contained a large number of granular tau oligomers, we found smaller-sized granules (data not shown).

Recent results have shown that inhibiting tau expression halfway during the neurodegeneration process in tau transgenic mice induces NFT formation without producing neuronal death (*5*). The findings presented here are not sufficient to resolve this issue. We do know, however, that tau overexpression in tau transgenic mice and in AD brains increases granular tau levels, ultimately leading to NFT formation and neuronal death (*18*−*21*). If the threshold concentration of granular tau that leads to neuronal death is higher than concentrations that lead to NFT formation, inhibiting tau expression could prevent neuronal death, even though NFTs are still generated. If this assumption is true, reducing oligomeric tau might be a promising therapy for various tauopathies, including those associated with aging. Nevertheless, the toxic nature of granular oligomeric tau aggregates needs to be further assessed.

ACKNOWLEDGMENT

We thank Dr. Hara for permitting us to use the NanoscopeIIIa, Drs. Kobayashi and Hayakawa for permitting us to use the Zetasizer, Mr. Usui and Miss Ohtsuki for MS spectroscopy, and Mr. Morishita for amino acid hydrolysis.

SUPPORTING INFORMATION AVAILABLE

Sarcosyl insoluble tau aggregates (Figure 1), temporal changes in in vitro tau aggregation (Figures 2 and 3), details of granular tau oligomer purification from human brain (Figure 4), and tau filament breakdown by continuous AFM imaging (Figure 5). This material is available free of charge via the Internet at http://pubs.acs.org.

REFERENCES

1. Braak, H., and Braak, E. (1997) Frequency of stages of Alzheimer-related lesions in different age categories, *Neurobiol. Aging 18*, 351−357.
2. Lee, V. M., Goedert, M., and Trojanowski, J. Q. (2001) Neurodegenerative tauopathies, *Annu. Rev. Neurosci. 24*, 1121−1159.
3. Ihara, Y. (2001) PHF and PHF-like fibrils: Cause or consequence? *Neurobiol. Aging 22*, 123−126.
4. Reed, L. A., Wszolek, Z. K., and Hutton, M. (2001) Phenotypic correlations in FTDP-17, *Neurobiol. Aging 22*, 89−107.
5. Santacruz, K., Lewis, J., Spires, T., Paulson, J., Kotilinek, L., Ingelsson, M., Guimaraes, A., DeTure, M., Ramsden, M., McGowan, E., Forster, C., Yue, M., Orne, J., Janus, C., Mariash, A., Kuskowski, M., Hyman, B., Hutton, M., and Ashe, K. H. (2005) Tau suppression in a neurodegenerative mouse model improves memory function, *Science 309*, 476−481.
6. Barghorn, S., and Mandelkow, E. (2002) Toward a unified scheme for the aggregation of tau into Alzheimer paired helical filaments, *Biochemistry 41*, 14885−14896.
7. Hasegawa, M., Smith, M. J., and Goedert, M. (1998) Tau proteins with FTDP-17 mutations have a reduced ability to promote microtubule assembly, *FEBS Lett. 437*, 207−210.
8. Friedhoff, P., Schneider, A., Mandelkow, E. M., and Mandelkow, E. (1998) Rapid assembly of Alzheimer-like paired helical filaments from microtubule-associated protein tau monitored by fluorescence in solution, *Biochemistry 37*, 10223−10230.
9. Yoshiike, Y., Tanemura, K., Murayama, O., Akagi, T., Murayama, M., Sato, S., Sun, X., Tanaka, N., and Takashima, A. (2001) New insights on how metals disrupt amyloid β-aggregation and their effects on amyloid-β cytotoxicity, *J. Biol. Chem. 276*, 32293−32299.
10. Maeda, S., Sahara, N., Saito, Y., Murayama, S., Ikai, A., and Takashima, A. (2006) Increased levels of granular tau oligomers: An early sign of brain aging and Alzheimer's disease, *Neurosci. Res. 54*, 197−201.
11. Kayed, R., Head, E., Thompson, J. L., McIntire, T. M., Milton, S. C., Cotman, C. W., and Glabe, C. G. (2003) Common structure of soluble amyloid oligomers implies common mechanism of pathogenesis, *Science 300*, 486−489.
12. George, A., and Wilson, W. W. (1994) Predicting protein crystallization from a dilute solution property, *Acta Crystallogr. D50*, 361−365.
13. Schweers, O., Schonbrunn-Hanebeck, E., Marx, A., and Mandelkow, E. (1994) Structural studies of tau protein and Alzheimer paired helical filaments show no evidence for β-structure, *J. Biol. Chem. 269*, 24290−24297.
14. Greenberg, S. G., and Davies, P. (1990) A preparation of Alzheimer paired helical filaments that displays distinct tau proteins by polyacrylamide gel electrophoresis, *Proc. Natl. Acad. Sci. U.S.A. 87*, 5827−5831.
15. Chirita, C. N., Congdon, E. E., Yin, H., and Kuret, J. (2005) Triggers of full-length tau aggregation: A role for partially folded intermediates, *Biochemistry 44*, 5862−5872.
16. Baskakov, I. V., Legname, G., Baldwin, M. A., Prusiner, S. B., and Cohen, F. E. (2002) Pathway complexity of prion protein assembly into amyloid, *J. Biol. Chem. 277*, 21140−21148.
17. Haroutunian, V., Davies, P., Vianna, C., Buxbaum, J. D., and Purohit, D. P. (2005) Tau protein abnormalities associated with the progression of alzheimer disease type dementia, *Neurobiol. Aging* (in press).
18. Tatebayashi, Y., Miyasaka, T., Chui, D. H., Akagi, T., Mishima, K., Iwasaki, K., Fujiwara, M., Tanemura, K., Murayama, M., Ishiguro, K., Planel, E., Sato, S., Hashikawa, T., and Takashima, A. (2002) Tau filament formation and associative memory deficit in aged mice expressing mutant (R406W) human tau, *Proc. Natl. Acad. Sci. U.S.A. 99*, 13896−13901.
19. Tanemura, K., Akagi, T., Murayama, M., Kikuchi, N., Murayama, O., Hashikawa, T., Yoshiike, Y., Park, J. M., Matsuda, K., Nakao, S., Sun, X., Sato, S., Yamaguchi, H., and Takashima, A. (2001) Formation of filamentous tau aggregations in transgenic mice expressing V337M human tau, *Neurobiol. Dis. 8*, 1036−1045.
20. Tanemura, K., Murayama, M., Akagi, T., Hashikawa, T., Tominaga, T., Ichikawa, M., Yamaguchi, H., and Takashima, A. (2002) Neurodegeneration with tau accumulation in a transgenic mouse expressing V337M human tau, *J. Neurosci. 22*, 133−141.
21. Brandt, R., Hundelt, M., and Shahani, N. (2005) Tau alteration and neuronal degeneration in tauopathies: Mechanisms and models, *Biochim. Biophys. Acta 1739*, 331−354.

BI061359O

J Neuropathol Exp Neurol

Vol. 66, No. 6
June 2007
pp. 469–480

ORIGINAL ARTICLE

Hematopoietic Prostaglandin D Synthase and DP_1 Receptor Are Selectively Upregulated in Microglia and Astrocytes Within Senile Plaques From Human Patients and in a Mouse Model of Alzheimer Disease

Ikuko Mohri, MD, PhD, Keiichi Kadoyama, PhD, Takahisa Kanekiyo, MD, Yo Sato, PhD, Kuriko Kagitani-Shimono, MD, PhD, Yuko Saito, MD, PhD, Kinuko Suzuki, MD, Takashi Kudo, MD, PhD, Masatoshi Takeda, MD, PhD, Yoshihiro Urade, PhD, Shigeo Murayama, MD, PhD, and Masako Taniike, MD, PhD

Abstract

Prostaglandin (PG) D_2 is produced in activated microglia by the action of hematopoietic PGD synthase (HPGDS) and plays important roles in neuroinflammation. Because the fact that neuroinflammation accelerates progression of Alzheimer disease (AD) has been documented, we investigated whether PGD_2 is also involved in the pathology of AD. Here, we report that the level of the mRNA of the receptor for PGD_2 (DP_1) was increased in AD brains compared with the level in non-AD brains. Immunocytochemical analysis showed HPGDS expression to be localized in the microglia surrounding senile plaques. In situ hybridization studies revealed that DP_1 mRNA was specifically localized in microglia and reactive astrocytes within senile plaques of AD brains. In the brain of Tg2576 mice, a model of AD, HPGDS and DP_1 proteins were mainly localized immunocytochemically in microglia and astrocytes in the plaques, and the levels of their mRNAs increased in parallel with amyloid β deposition. These results indicate that PGD_2 may act as a mediator of plaque-associated inflammation in AD brain and may explain the pharmacologic mechanisms underlying the favorable response of patients with AD to nonsteroidal anti-inflammatory drugs.

Key Words: Alzheimer disease, Amyloid β, Gliosis, Neuroinflammation, Nonsteroidal anti-inflammatory drugs (NSAIDs), Prostanoid, Tg2576 mouse.

INTRODUCTION

Alzheimer disease (AD) is the most common form of dementia. The cognitive decline in patients with AD is associated with neuronal degeneration, the appearance of neurofibrillary tangles, and the formation of senile plaques (1). It has been reported that inflammatory responses, including the production of proinflammatory cytokines and prostaglandins by activated microglia and astroglia, play important roles in the pathology of AD (2–5). Senile plaques arise from the excessive accumulation, aggregation, and deposition of amyloid β (Aβ) peptide, which triggers the activation of microglia and astrocytes around the senile plaques. Tg2576 mice overexpressing human APP695 with the "Swedish" mutation (a murine model of AD) develop memory deficits and senile plaques as they age (6). These animals show a rapid increase in Aβ deposition starting around 6 months and amyloid plaques beginning at 9 to 12 months (7).

We recently reported that activated microglia express hematopoietic prostaglandin (PG) D synthase (HPGDS) and that PGD_2 produced by HPGDS promotes neuroinflammation in a mouse model of Krabbe disease (8). These discoveries

From Department of Mental Health and Environmental Effects Research (IM, M. Taniike), The Research Center for Child Mental Development, Osaka University Graduate School of Medicine, Suita, Osaka, Japan; Department of Developmental Medicine (Pediatrics) (IM, TK, KK-S, M. Taniike), Osaka University Graduate School of Medicine, Suita, Osaka, Japan; Department of Molecular Behavioral Biology (IM, KK, Y. Sato, YU), Osaka Bioscience Institute, Suita, Osaka, Japan; Department of Pathology and Laboratory Medicine (IM, KS), School of Medicine, University of North Carolina at Chapel Hill, Chapel Hill, North Carolina; Departments of Neuropathology and Pathology (Y. Saito, SM), Tokyo Metropolitan Geriatric Hospital, Itabashi-ku, Tokyo, Japan; and Division of Psychiatry and Behavioral Proteomics (TK, M. Takeda), Department of Post-Genomics and Diseases, Course of Advanced Medicine, Osaka University, Graduate School of Medicine, Suita, Osaka, Japan.

Drs. Mohri, Kadoyama, and Kanekiyo contributed equally to this work.

Drs. Urade, Murayama, and Taniike contributed equally in supervising this project.

Send correspondence and reprint requests to: Masako Taniike, MD, PhD, Department of Mental Health and Environmental Effects Research, The Research Center for Child Mental Development, Osaka University Graduate School of Medicine, 2-2, D-5, Yamadaoka, Suita, Osaka 565-0871, Japan; E-mail: masako@ped.med.osaka-u.ac.jp

This study was supported in part by research grants from the Ministry of Education, Culture, Sports, Science, and Technology of Japan (M. Taniike); the Osaka Medical Research Foundation for Incurable Diseases (M. Taniike), Japan Science and Technology Corporation (YU); Takeda Science Foundation (YU); Aid for Scientific Research on Priority Areas Advanced Brain Science Project from the Ministry of Education, Culture, Sports, Science, and Technology of Japan (SM, Y. Saito); Aid for Longevity Sciences from the Ministry of Health, Labor, and Welfare (SM); and Aid for Long-Term Comprehensive Research on Age-Associated Dementia from Tokyo Metropolitan Institute of Gerontology (SM), and Osaka City.

prompted us to clarify whether PGD_2 is also involved in the plaque-associated inflammation in the AD brain. A determination of the mRNA contents of all known brain prostanoid synthases and receptors showed that HPGDS and DP1 mRNAs were selectively expressed to a higher level in AD brains compared with their levels in age-matched control patients. This overexpression was localized to reactive astrocytes and microglia closely associated with senile plaques, suggesting that HPGDS/PGD_2/DP_1 signaling may accelerate chronic local inflammation around plaques in AD. We also found that HPGDS and DP_1 mRNAs were selectively expressed in reactive astrocytes and microglia closely associated with senile plaques in the AD brains and brains of Tg2576 mouse. Our findings suggest that HPGDS/PGD_2/DP_1 signaling may accelerate chronic local inflammation around senile plaques in the AD brain.

MATERIALS AND METHODS

Human Tissue Source

Human brain tissues were obtained from Tokyo Metropolitan Brain Bank for Aging Research according to the neuropathologic protocols described elsewhere (9). We obtained tissue fresh at autopsy and stored it at −80°C, and, to avoid RNA degradation, we selected samples with as short a postmortem interval before autopsy as possible. The storage period was 2 to 32 months and 2 to 31 months for AD and control brains, respectively, and the storage period was not significantly different between the 2 groups.

Fifteen brains each from AD patients and control patients without clinicopathologic evidence of AD were the basis of the present work. The diagnosis of AD was based on the following criteria: 1) clinical dementia rating of ≥1 (10); 2) the topographical distribution of senile plaques matching Braak stage C; and 3) of neurofibrillary tangles equal to or above stage IV, as reported elsewhere (9). The selection criterion for control patients was a clinical dementia rating score of 0, senile plaque stage 0 or A, and a neurofibrillary tangle stage lower than stage II. The profiles of AD and control patients are listed in Table 1. Subjects with AD were 70 to 93 years old (82.6 years on average), and the postmortem delay ranged from 1.5 to 17 hours (average of 8.5 hours). The age of non-AD control patients was 71 to 91 years (79.5 on average), and the postmortem delay was 2.3 to 14.8 hours (average of 12.1 hours).

The tissues were either snap-frozen in liquid nitrogen or powdered dry ice or immediately fixed in 4% paraformaldehyde (Sigma, St. Louis, MO) for 2 days and processed into paraffin blocks. Paraffin or frozen sections of 6-μm thickness from the frontal cortex and the hippocampus were cut with a cryostat (CM1850; Leica Microsystems, Wetzlar, Germany) and microtome (RM 2035; Leica), and used for immunohistochemical studies. Snap-frozen tissues, that were en face to the paraffin sections, were also used for quantitative reverse transcriptase (RT)-polymerase chain reaction (PCR) analysis of mRNA expression. The frontal cortex was selected for this purpose, because the difference in the number of senile plaques was most prominent there between AD and control groups. This study was approved by the institutional review boards of Osaka University Graduate School of Medicine, Tokyo Metropolitan Geriatric Hospital, Tokyo Metropolitan Institute of Gerontology, and Osaka Bioscience Institute.

Mice

All animal experiments were performed in accordance with Japanese law for the protection of experimental animals and conformed to the regulations issued by the National Institutes of Health and the Society for Neuroscience. Homozygous Tg2576 mice were purchased from Taconic (Hudson, NY) and maintained by interbreeding.

Quantitative Reverse Transcriptase-Polymerase Chain Reaction Analysis of mRNA

By quantitative RT-PCR analysis, we determined the mRNA contents of enzymes involved in prostanoid synthesis, including cyclooxygenase (COX)-1, COX-2, HPGDS, lipocalin-type PGD synthase (L-PGDS), microsomal PGE synthases (mPGES-1 and mPGES-2), cytosolic PGE synthase (cPGES), PGF synthase, prostacyclin synthase, thromboxane (TX) A synthase, and those of prostanoid receptors for PGD_2 (DP_1 and DP_2), PGE_2 (EP_1, EP_2, EP_3, and EP_4), $PGF_{2\alpha}$ (FP), PGI_2 (IP), and TXA_2 (TP), as well as the mRNA content of cytosolic phospholipase A_2 ($cPLA_2$) and peroxisome proliferator-activated receptor (PPAR)-γ. After removal of the pia-arachnoid membrane, total RNA was prepared from the frontal cortex of 17 AD patients and 12 control patients by using ISOGEN (Nippon Gene, Tokyo, Japan) according to the manufacturer's instructions. In the mouse model, 3 each of Tg2576 and age-matched wild-type mice at ages 6 months, 1 year, and 2 years were subjected to quantitative RT-PCR for determination of COX-1, COX-2, HPGDS, DP_1, and DP_2 mRNA levels. All primers were synthesized by Sigma-Aldrich Japan (Tokyo, Japan). First-strand cDNAs were synthesized from 1 μg of total RNA by using avian myeloblastosis virus reverse transcriptase (Takara, Kyoto, Japan) and oligo dT-adaptor primer (Takara) at 50°C for 40 minutes after denaturation at 72°C for 3 minutes. The cDNA was amplified by use of a real-time PCR LightCycler system (Roche Diagnostics, Indianapolis, IN), a LightCycler-FastStart DNA Master SYBR Green I (Roche Diagnostics), and gene-specific primers under the following conditions: an initial denaturation at 94°C for 10 minutes, followed by 40 cycles of denaturation at 94°C for 15 seconds, annealing for 5 seconds, and extension at 72°C for 10 seconds. The oligonucleotide primers and annealing temperatures used are shown in Table 2. All oligonucleotide primers were synthesized by Sigma Genosys Japan (Tokyo, Japan). PCR products were evaluated by melting-curve analysis following the manufacturer's instructions, checked after agarose gel electrophoresis, and sequenced. All values were corrected with reference to the value for glyceraldehyde-3-phosphate dehydrogenase (G3PDH), used as an internal standard.

Immunocytochemistry

Rabbit polyclonal antibodies against human HPGDS, L-PGDS, and mPGES-1 (11), and rabbit polyclonal

TABLE 1. Clinicopathologic Features of the Patients

Patient	Age	Sex	Neuropathologic Diagnosis	SP	NFT	CERAD	Postmortem Interval (hours)	Cause of Death
C1	91	F	Unremarkable	A	II	Normal	13:25	DIC, Heart failure
C2	83	M	Unremarkable	0	I	Normal	17:43	AMI
C3	82	M	Unremarkable	A	I	Normal	12:16	COPD
C4	81	M	Unremarkable	0	I	Normal	2:14	MDS, congestive heart failure
C5	80	M	Unremarkable	0	II	Normal	8:50	Hepatocellular carcinoma
C6	79	F	Unremarkable	A	I	Normal	2:52	AAA, COPD
C7	78	M	Unremarkable	0	II	Normal	2:30	COPD, sudden death
C8	78	M	Unremarkable	0	I	Normal	9:35	Sepsis
C9	78	F	Unremarkable	A	I	Normal	2:39	Sepsis
C10	77	M	Unremarkable	0	I	Normal	10:25	Lung cancer (small cell carcinoma)
C11	76	M	Unremarkable	A	II	Normal	5:14	Lung cancer (small cell carcinoma)
C12	71	M	Unremarkable	0	I	Normal	13:54	Severe pneumonia, sepsis
AD1	93	M	AD	C	V	Definite	1:47	Leiomyosarcoma of stomach, abdominal dissemination
AD2	91	M	AD	C	IV	Definite	9:40	Carcinoma of the bile duct
AD3	88	F	AD	C	VI	Definite	5:25	AMI, sepsis
AD4	87	M	AD	C	VI	Definite	3:17	Lung cancer
AD5	87	F	AD	C	V	Definite	16:56	MRSA sepsis
AD6	85	F	AD	C	VI	Definite	16:40	Ileus, pneumonia
AD7	84	M	AD	C	V	Definite	9:50	Pneumonia, ileus
AD8	84	F	AD	C	V	Definite	8:41	Cholecystitis
AD9	84	F	AD	C	IV	Definite	9:35	Congestive heart failure, OMI
AD10	82	F	AD	C	VI	Definite	4:14	Perforation of gastric ulcer
AD11	82	F	AD	C	V	Definite	8:53	Sudden death
AD12	81	M	AD	C	IV	Definite	12:57	AMI, septal perforation
AD13	81	M	AD	C	VI	Definite	6:00	Pulmonary emphysema, respiratory failure
AD14	76	M	AD	C	VI	Definite	15:47	Sepsis, early gastric cancer
AD15	75	M	AD	C	VI	Definite	9:54	Pneumonia
AD16	74	M	AD	C	VI	Definite	5:12	Pneumonia, DIC
AD17	70	M	AD	C	V	Definite	11:42	Hodgkin lymphoma, pneumonia

The diagnosis of AD was based on a clinical dementia rating (CDR) of ≥1, topographical distribution of senile plaques (SP) matching Braak stage C, and that of neurofibrillary tangles (NFTs) equal to or above stage IV (9). The selection criterion for control patients was a CDR score of 0, senile plaque stage 0 or A, and an NFT stage lower than stage II.

AAA, abdominal aortic aneurysm; AD, Alzheimer disease; AMI, acute myocardial infarction; CERAD, Consortium to Establish A Registry for Alzheimer's Disease; COPD, chronic obstructive pulmonary disease; DIC, disseminated intravascular coagulation; MDS, myelodysplastic syndrome; MRSA, methicillin-resistant *Staphylococcus aureus*; OMI, occlusive mesenteric ischemia.

(0.1 μg/mL) and rat monoclonal (0.2 μg/mL) anti-mouse HPGDS antibodies (12) were raised and purified in Osaka Bioscience Institute. The specificity of each antiserum (1:1000 dilution) was confirmed by the disappearance of immunoreactivity after incubation of the antiserum with an excess amount of the corresponding purified recombinant immunogen. The other primary antibodies used in this study were as follows: anti-cow glial fibrillary acidic protein (GFAP) (1:5000 dilution; DakoCytomation, Glostrup, Denmark) for astrocytes; anti-human CD68 antibody (1:100 dilution; DakoCytomation) and anti-Iba1 (a generous gift of Dr. Shinichi Kousaka, National Center of Neurology and Psychiatry, Japan) for microglia/macrophages; and anti-human Aβ (11-28) antibody (1:100 dilution; IBL, Gunma, Japan) for detecting amyloid plaques.

Tg2576 and control mice were used for immunocytochemical analysis. Under deep ether anesthesia, the mice were perfused via the heart with physiologic saline, followed by 4% paraformaldehyde in 0.1 M sodium phosphate (pH 7.4) for 10 minutes. The brains were removed and postfixed in the same fixative overnight. Coronal slices were taken and routinely embedded in paraffin. Additionally, 2 each of Tg2576 and control mice were perfused with physiologic saline only and processed for the preparation of fresh-frozen sections. Both paraffin and frozen sections (5-μm thickness) were mounted on 3-aminopropyltriethoxysilane-coated slides.

Deparaffinized sections were preincubated with 0.3% H_2O_2 (Wako, Osaka, Japan) in methanol followed by PBS containing 0.2% Triton X-100 (Nakarai Tesque, Kyoto, Japan). After pretreatment with 0.1% trypsin (Sigma) at 37°C for 15 minutes, they were sequentially incubated with primary antibody, biotinylated secondary antibody (2 μg/mL; Vector Laboratories, Burlingame, CA), and avidin-biotin-complex (ABC) by using an ABC elite system (Vector Laboratories) according to the manufacturer's protocol.

For double immunostaining, deparaffinized sections were incubated at 4°C overnight with either anti-GFAP or anti-CD68 antibody together with rabbit anti-human HPGDS

TABLE 2. Primer Sequences and Annealing Temperatures Used for Quantitative Reverse Transcriptase-Polymerase Chain Reaction Analysis

	Primer	Primer Sequence	Annealing Temperature (°C)
Human			
HPGDS	Forward	5′-GAATAGAACAAGCTGACTGGC-3′	57
	Reverse	5′-AGCCAAATCTGTGTTTTTGG-3′	
L-PGDS	Forward	5′-CAGGAAAAACCAGTGTGAGACC-3′	57
	Reverse	5′-AGAGGGTGGCCATGCGGAAG-3′	
mPGES-1	Forward	5′-CTGCTGGTCATCAAGATGTACG-3′	59
	Reverse	5′-ACACACCGTGGCCTACCTGGG-3′	
mPGES-2	Forward	5′-TACCAGTACAAGACGTGTCCCTTC-3′	56
	Reverse	5′-GGTAGTAGGTGATGATCTCTTCCAG-3′	
cPGES	Forward	5′-TACATTCAGTTGTCTCGGAGGAAG-3′	56
	Reverse	5′-ATCATCTGCTCCATCTACTTCTGG-3′	
PGFS	Forward	5′-GGCAGTGTGAAGAGAGAAGACATA-3′	56
	Reverse	5′-AATCCTGCATCCTTACACTTCTCC-3′	
DP_1	Forward	5′-CCTCTGAAGAAGCAGAAGACCT-3′	56
	Reverse	5′-CCTCAGCTTACCACAGAGTGA-3′	
DP_2	Forward	5′-CTCCTCCATCTTCTTTCTCAACA-3′	56
	Reverse	5′-TTCAGGAGCAGCACATTGTAGTA-3′	
EP_1	Forward	5′-AACCTGAGCCTGGCGGGCGAGGCGA-3′	55
	Reverse	5′-AGAAGACCATGCAGCCGCCCAGGAA-3′	
EP_2	Forward	5′-GTGCGAGTATTCGTCAACCAGT-3′	57
	Reverse	5′-TGACATGGCAGAAGATGTCCTT-3′	
EP_3	Forward	5′-GACAGTCACCTTTTCCTGCAAC-3′	57
	Reverse	5′-CCAGGCGAACAGCTATTAAGAA-3′	
EP_4	Forward	5′-CCTGAGAAAGACAGTGCTCAGTAA-3′	55
	Reverse	5′-CTGAGGTCTCTGATATTCGCAAAG-3′	
FP	Forward	5′-ATTTAGACAGAAGTCCAAGGCATC-3′	56
	Reverse	5′-AACAAGCACACACCACTTAACATC-3′	
G3PDH	Forward	5′-TGAACGGGAAGCTCACTGG-3′	60
	Reverse	5′-TCCACCACCCTGTTGCTGTA-3′	
Mouse			
COX-1	Forward	5′-AGATAATCTGGAACGACAGTATCACC-3′	60
	Reverse	5′-CATAGTCCACCAGCATAGAAGTGTTA-3′	
COX-2	Forward	5′-AACTGTACCCTGCCCTGCTGGTGGAAAA-3′	59
	Reverse	5′-AGATGACATTAACCCTACAGTACTAATC-3′	
HPGDS	Forward	5′-GAATAGAACAAGCTGACTGGC-3′	57
	Reverse	5′-AGCCAAATCTGTGTTTTTGG-3′	
DP_1	Forward	5′-TTTGGGAAGTTCGTGCAGTACT-3′	56
	Reverse	5′-GCCATGAGGCTGGAGTAGA-3′	
DP_2	Forward	5′-TGGCCTTCTTCAACAGCGT-3′	56
	Reverse	5′-ACGCAGTTGGGGAATTCG-3′	
G3PDH	Forward	5′-TGAACGGGAAGCTCACTGG-3′	60
	Reverse	5′-TCCACCACCCTGTTGCTGTA-3′	

COX, cyclooxygenase; cPGES, cytosolic PGES; DP_1 and DP_2, prostanoid receptors for PGD_2; EP_1, EP_2, EP_3, and EP_4, prostanoid receptors for PGE_2; FP, prostanoid receptor for $PGF_{2\alpha}$; G3PDH, glyceraldehyde-3-phosphate dehydrogenase; HPGDS, hematopoietic prostaglandin (PG) D synthase; L-PGDS, lipocalin-type PGD synthase; mPGES, microsomal PGE synthase; PGFS, PGF synthase.

antiserum. The sections were then reacted with alkaline phosphatase-conjugated anti-mouse IgG antibody (2 μg/mL; Aurora, Cambridge, UK) and biotin-conjugated anti-rabbit IgG antibody (Vector Laboratories), followed by ABC. The reaction products of horseradish peroxidase and alkaline phosphatase activities were visualized with diaminobenzidine (Dotite, Kumamoto, Japan) and naphthol AS-BI phosphate (Sigma) coupled to hexazotized new fuchsin (Merck, Darmstadt, Germany), respectively, as substrates.

All sections were analyzed, and images were obtained with an Olympus BX51 microscope (Olympus, Tokyo, Japan) equipped with a DP50 digital camera. The digital images were adjusted to an appropriate figure size required but were otherwise not processed.

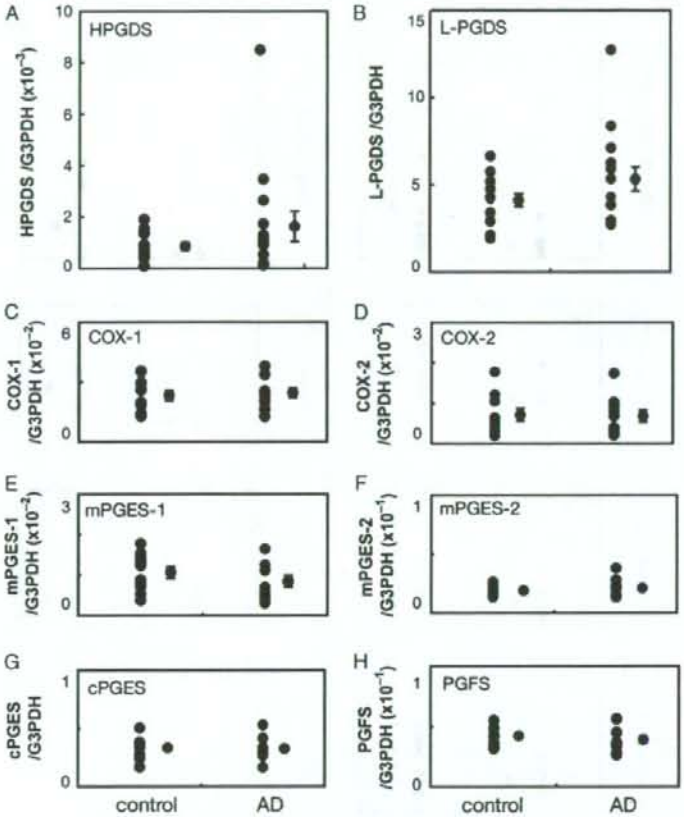

FIGURE 1. (A–H) Expression of prostaglandin synthase mRNA in the frontal cortex of AD (n = 17) and control brains (n = 12), as evaluated by quantitative RT-PCR analysis. The numbers of copies relative to those of G3PDH are shown. The mean values and SE are indicated by the crossbars. AD, Alzheimer disease; COX, cyclooxygenase; cPGES, cytosolic PGES; HPGDS, hematopoietic prostaglandin (PG) D synthase; G3PDH, glyceraldehyde-3-phosphate dehydrogenase; L-PGDS, lipocalin-type PGD synthase; mPGES, microsomal PGE synthase; PGFS, PGF synthase.

In Situ Hybridization

In situ hybridization was performed by using a digoxigenin (DIG)-anti-DIG technique. For preparation of the human DP_1 riboprobe, a 484-base pair fragment was amplified by use of FastStart Taq DNA polymerase (Roche Diagnostics) with human DP_1-specific primers (forward, 5′-GGGGTACTCTGTGCTCTACTCCAG-3′ and reverse, 5′-ACTGGATTCCATGTTAGTGGAATTG-3′), subcloned into pGEM-T Easy vector (Promega, Madison, WI), and converted into the corresponding RNA. Five-micrometer-thick cryosections were fixed in 10% formalin (Wako) for 1 hour and hybridized at 58°C for 16 hours with the DIG-labeled riboprobe for DP_1 in 50% formamide (Wako), 5 × saline sodium citrate, 5 × Denhardt's solution, 0.25 mg/mL yeast tRNA, and 0.5 mg/mL herring sperm DNA. After the sections had been washed with PBS, the DIG-labeled RNA was detected by using a Genius DNA labeling and detection kit (Roche Diagnostics) according to the manufacturer's protocol.

For identification of DP_1-expressing cells, the sections were reacted with the DP_1-specific riboprobe and then immunostained with either anti-human GFAP antibody, anti-human CD68 antibody, or anti-human Aβ (11-28) antibody detected by using either immunofluorescence or immunoperoxidase. For fluorescence labeling, a biotinylated riboprobe was used in place of the DIG-labeled riboprobe. For double immunofluorescence, we confirmed the colocalization by omitting 1 of the first antibodies during the process.

Primary Cultures of Mouse Microglia and Astrocytes

We prepared primary cultures of microglia from wild-type mouse brains at postnatal day 1. Cerebral cortices were dissected, and the leptomeninges were completely removed.

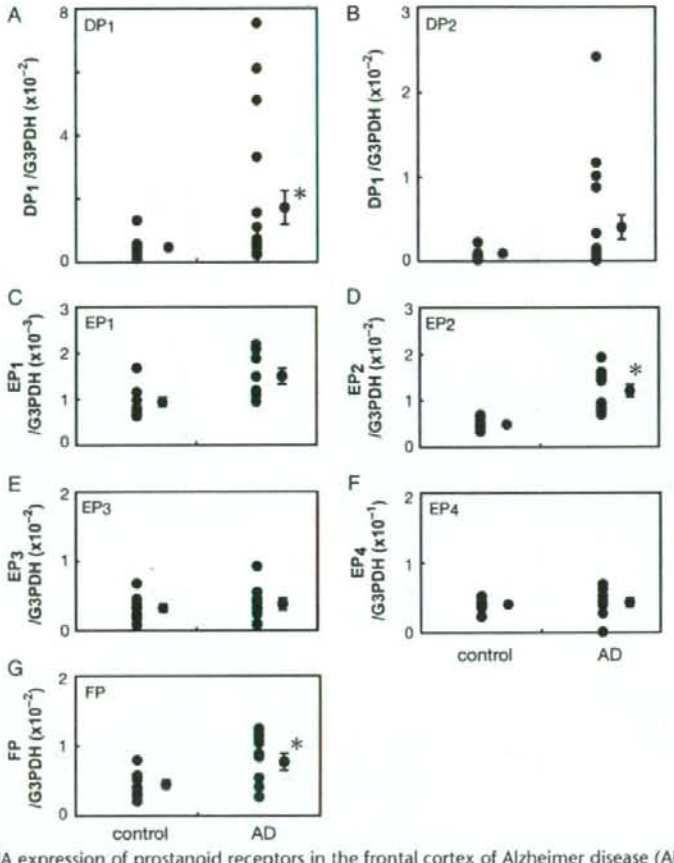

FIGURE 2. (A–G) mRNA expression of prostanoid receptors in the frontal cortex of Alzheimer disease (AD) (n = 17) and control brains (n = 12), as determined by quantitative RT-PCR analysis. The numbers of copies relative to glyceraldehyde-3-phosphate dehydrogenase (G3PDH) are shown. The mean values and SE are indicated by the crossbars. *, $p < 0.05$.

The tissues were minced, suspended in PBS (GIBCO, Grand Island, NY) containing 0.05% trypsin (GIBCO) and 0.01% DNase I (Sigma), and then incubated for 10 minutes at 37°C. After incubation and centrifugation, the cell pellets were washed 3 times with PBS. The cells were then filtered through a 75-μm nylon mesh, centrifuged, suspended in Dulbecco's modified Eagle's medium (Nakalai Tesque) containing 10% fetal bovine serum (JRH Biosciences, Lenexa, KS), 100 IU/mL penicillin (GIBCO), and 100 μg/mL streptomycin (GIBCO), and transferred to culture dishes. For microglial cultures, the medium was changed to Dulbecco's modified Eagle's medium containing 10% fetal bovine serum after a 24-hour culture period. This medium was exchanged for fresh medium twice weekly thereafter. The supernatants including microglial cells were collected and subcultured at 1×10^5 cells/well (6-well plate). After incubation in Dulbecco's modified Eagle's medium without fetal bovine serum for 6 hours, the microglia were stimulated by the addition of Aβ (1-40) (Peptide Institute, Osaka, Japan) for 24 hours. After the cells had been washed with PBS, RNA was extracted from them and subjected to quantitative RT-PCR.

Data Analysis

The difference of means among groups of data was analyzed by analysis of variance. Statistical significance was established at the level of $p < 0.05$ or 0.01.

RESULTS

Expression of Prostanoid-Producing Enzymes in Alzheimer Disease Brains

Using the frontal cortex obtained from AD and control patients, we examined the mRNA expression level of all enzymes involved in prostanoid synthesis. Quantitative

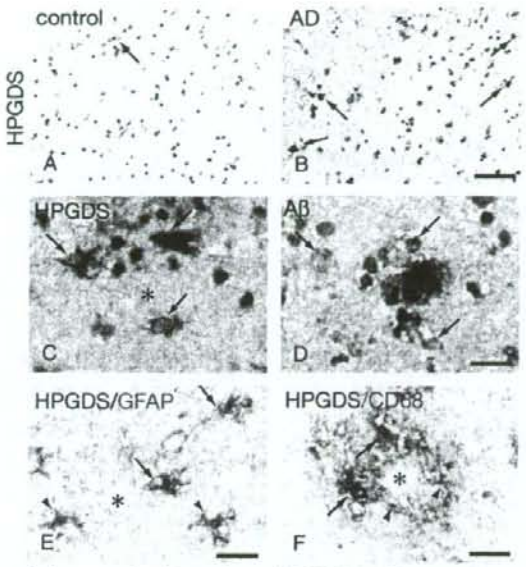

FIGURE 3. Expression of hematopoietic prostaglandin synthase (HPGDS) in Alzheimer disease (AD) and control brains. In the following panels, asterisks indicate the presence of senile plaques. **(A, B)** Immunohistochemical analysis of HPGDS in control **(A)** and AD **(B)** brains. Arrows point to HPGDS-positive cells. Scale bar = 50 μm. **(C, D)** Immunostaining for HPGDS **(C)** and amyloid β (Aβ) **(D)** associated with the senile plaques in an AD brain. The same cells in the serial sections are indicated by arrows. Scale bar = 20 μm. **(E, F)** Double immunostaining for HPGDS (purple) and glial fibrillary acidic protein (GFAP) (pink, **E**) or CD68 (pink, **F**) in an AD brain. HPGDS-positive/GFAP- **(E)** or CD68-positive **(F)** and HPGDS-negative/GFAP- **(E)** or CD68-positive **(F)** cells are indicated by arrows and arrowheads, respectively. Scale bar = 20 μm.

RT-PCR analysis revealed the mRNA levels of HPGDS (Fig. 1A) and L-PGDS (Fig. 1B) to be elevated in AD brains compared with those of the control brains. However, the mRNA levels of other prostanoid-producing enzymes including COX-1 and -2 (Fig. 1C, D), PGESs including mPGES-1, mPGES-2, and cPGES (Fig. 1E–G), PGF synthase (Fig. 1H), and TXA synthase (data not shown), as well as the mRNA level of $cPLA_2$ (data not shown), were similar between control and AD brains. Prostacyclin synthase mRNA was not detected in either AD or control samples (data not shown).

Increased DP_1 Expression in Alzheimer Disease Brains

Next, we examined the mRNA expression level of all prostanoid receptors thus far identified (Fig. 2) and found that the expression of DP_1 was significantly upregulated in AD brains as compared with that in control brains (Fig. 2A). In 6 of the 17 AD patients, the mRNA level was higher than 2 SD from the mean of control brains, and these values were 2.5- to 16-fold greater than this mean. The mRNA level of DP_2, which is another PGD_2 receptor, was also increased, but not significantly, in AD brains (Fig. 2B). In contrast, the mRNA levels of other prostanoid receptors were almost the same between the 2 groups (Fig. 2C–G) except for the approximately 2-fold increases in EP_2 (Fig. 2D) and FP (Fig. 2G) in AD brains. In addition, the mRNA level of PPARγ, which is a nuclear receptor for PGD_2 metabolites (13), was not significantly different between AD and control brains (data not shown).

Expression of Hematopoietic Prostaglandin D Synthase and DP_1 Is Associated with Senile Plaques in Alzheimer Disease Brains

Because the mRNA levels of HPGDS and DP_1 mRNA were increased in AD brains, as judged from the results of RT-PCR analysis, we investigated the cellular localization of these messages.

Immunocytochemical analysis revealed that anti-HPGDS-immunoreactive cells were greater in number in the AD brain than in the control brain (Fig. 3A, B). Serial immunostaining for HPGDS and Aβ revealed that HPGDS-positive cells were closely associated with Aβ-positive senile plaques (Fig. 3C, D) in the frontal cortex and the hippocampus. HPGDS-positive cells were frequently recognized in relatively small-sized plaques accompanied by activated microglia (Fig. 3B, C) but not in the large "burned out class" of plaques (data not shown). Double immunocytochemical staining revealed that HPGDS was localized in GFAP-positive reactive astrocytes (Fig. 3E) and in CD68-positive microglia (Fig. 3F) associated with the senile plaques, suggesting that HPGDS expression was upregulated

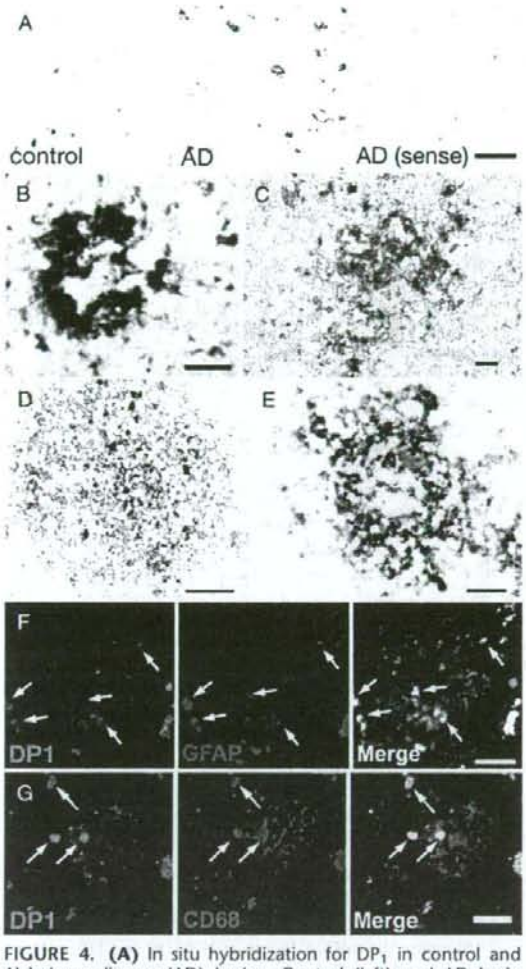

FIGURE 4. **(A)** In situ hybridization for DP_1 in control and Alzheimer disease (AD) brains. Control (left) and AD brain (middle) sections were incubated with antisense riboprobe. Another AD brain section was incubated with sense riboprobe (right). Scale bar = 100 μm. **(B, C)** In situ hybridization for DP_1 (purple) and immunocytochemistry for amyloid β (Aβ) (pink) in an AD brain. The DP_1-positive cells are uniformly intermingled with Aβ immunoreactivity in the senile plaque **(B)**, and a large-sized DP_1-negative senile plaque is shown **(C)**. Scale bar = 20 μm. **(D, E)** Double staining by in situ hybridization for DP_1 (purple) and immunocytochemistry for glial fibrillary acidic protein (GFAP) (brown, **D**) or CD68 (brown, **E**). Scale bar = 50 μm. **(F, G)** Double fluorescence labeling for DP_1 (green) and GFAP (red, **F**) or CD68 (red, **G**). Double-positive cells are indicated by arrows. Scale bar = 30 μm.

in reactive astrocytes and microglia within the senile plaques. Immunocytochemical analysis revealed that L-PGDS-expressing cells having the same morphologic characteristics as oligodendrocytes, as reported previously (14), were increased in number and were more intensely stained in AD than in control brains; however, the distribution of L-PGDS-positive oligodendrocytes was almost ubiquitous and seemingly unrelated to that of senile plaques (data not shown). mPGES was localized in some neurons of both AD and control brains, but there was no significant difference in intensity of staining or in the number of immunoreactive neurons between the 2 (data not shown).

Upregulation of DP_1 mRNA in AD brains was confirmed by in situ hybridization with a DP_1-specific antisense riboprobe, because antibody specific for human DP_1 is still unavailable. DP_1 mRNA was hardly detected in the control brain (Fig. 4A); however, high signal density was detected in AD brains (Fig. 4A). When we hybridized the sections with the DIG-labeled antisense riboprobe in the presence of a 500-fold excess of nonlabeled antisense riboprobe or with sense riboprobe, no signal was observed in either control or AD brain sections (Fig. 4A, sense). Double labeling for Aβ and DP_1 hybridization revealed that the distribution of the DP_1 signal was closely associated with Aβ immunoreactivity (Fig. 4B). However, the intensity of the DP_1 signal differed among the senile plaques; and the signal was less preferentially observed in large-sized senile plaques (Fig. 4C). Furthermore, double staining with antibodies against glial markers revealed that the DP_1 signal was localized in GFAP-positive reactive astrocytes (Fig. 4D, F) and CD68-positive microglia (Fig. 4E, G) within senile plaques, similar to the distribution of HPGDS shown in Figure 3E and F. These results indicate that expression of HPGDS and DP_1 was increased in reactive astrocytes and microglia within the senile plaques in AD brain and suggest that PGD_2 produced by HPGDS exerts its function through binding to DP_1 in a paracrine or autocrine manner. The preferential expression of these PGD_2-related molecules in the small-sized senile plaques suggests the contribution of PGD_2 to neuroinflammation in the early phase of plaque evolution.

Upregulation of Hematopoietic Prostaglandin D Synthase and DP_1 Expression in Tg2576 Mouse Brain

Next we examined the Tg2576 mouse brain to clarify the relevancy of our findings on human AD brains. In 2-year-old mice, there were numerous amyloid plaques in the cortex of Tg2576 brains (Fig. 5A) but not in that of the wild-type mouse brain (Fig. 5B). The results of the combination of Congo red staining and immunocytochemistry for Iba1, a marker for activated microglia, are shown in Figure 5C and D. Surrounding the amyloid plaques were many Iba1-positive activated microglia (Fig. 5D, arrowheads), which were not seen in the wild-type control. Double labeling with Congo red and anti-GFAP showed that fibers from activated astrocytes surrounded and enclosed amyloid plaques (Fig. 5E, F). These findings indicate that inflammatory responses such as microglial activation and astrogliosis were remarkable around early amyloid plaques in the Tg2576 mouse brain.

Next we investigated the localization of HPGDS and DP_1 in the Tg2576 mouse brain. As in the case of the human

AD brains, HPGDS-positive microglia were common in relatively small plaques (Fig. 5G) but not in the large burned out class of plaques (Fig. 5H). HPGDS and Iba1 double immunofluorescence revealed that HPGDS was expressed in a certain number of Iba1-positive activated microglia (Fig. 5I). DP_1 and GFAP double immunofluorescence revealed that DP_1 was expressed on the astrocytic processes close to the amyloid plaques (Fig. 5J).

Quantitative RT-PCR was performed to evaluate the level of PGD_2-related molecules in Tg2576 mouse brains and age-matched controls at the age of 6 months, 1 year, and 2 years. The expression of COX-1 mRNA was not different between Tg2576 and control mice (Fig. 6A), but that for COX-2 was higher in the Tg2578 mouse starting from the age of 6 months (Fig. 6B). The level of HPGDS mRNA was the same between Tg2576 and wild-type controls until they reached 2 years of age, at which time its level was 1.5 times higher in the Tg2576 mice than in the controls (Fig. 6C). The level of DP_1 mRNA progressively increased in the Tg2576 mouse brain and reached a level 5-times higher than that in the control mice at the age of 2 years (Fig. 6D). In the case of DP_2, its mRNA level progressively increased starting before the age of 1 year compared with that of the age-matched controls (Fig. 6E). These lines of evidence show that HPGDS and DP_1 expression was associated with the small senile plaques and that the increase in DP_2 receptors was more marked than that of HPGDS in the mouse model as in human AD.

To examine whether Aβ could directly stimulate the production of HPGDS in microglia, we performed an in vitro study using primary cultures of microglia obtained from normal neonatal mouse brains. We measured the level of HPGDS mRNA in these cultures before and after stimulating the cells with Aβ(1-42) at concentrations from 0 to 1000 nM. As shown in Figure 6F, the level of HPGDS mRNA did not increase when a 1 nM concentration of Aβ(1-42) was tested but did significantly increase when a 10 nM concentration or higher was used. However, no

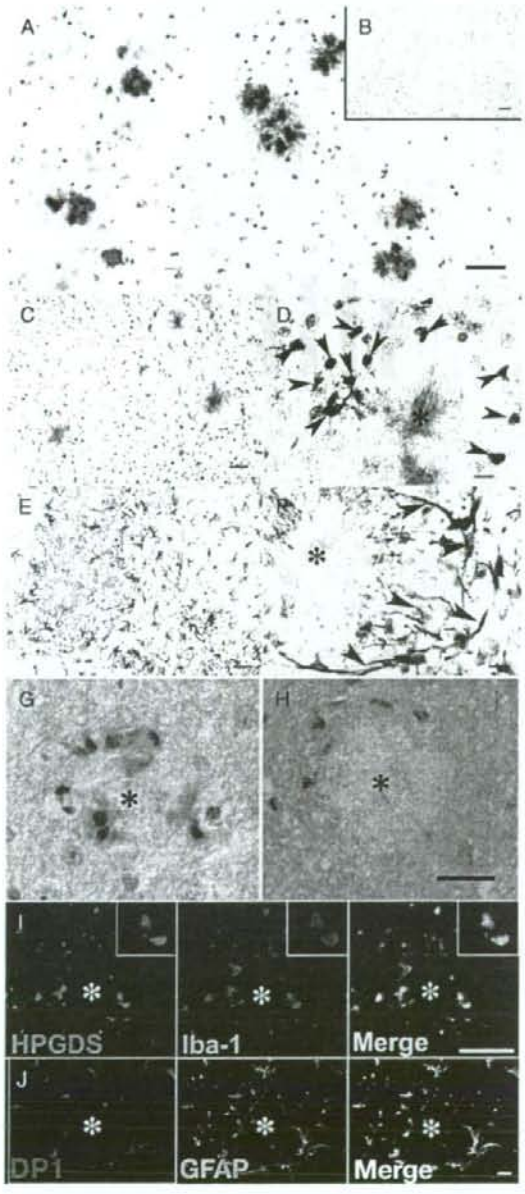

FIGURE 5. **(A, B)** Amyloid β (Aβ) immunostaining of primary motor cortex of Tg2576 **(A)** and wild-type **(B)** brains from 2-year-old mice. Scale bar = 200 μm. **(C, D)** Combination of Congo red staining (pink) and Iba1 immunocytochemistry (brown) in a Tg2576 mouse brain. **(D)** The arrowheads and asterisk indicate Iba1-positive activated microglia and an amyloid plaque, respectively. Scale bars = **(C)** 200 μm; **(D)** 20 μm. **(E, F)** Combination of Congo red staining (pink) and glial fibrillary acidic protein (GFAP) immunocytochemistry (brown) in a Tg2576 mouse brain. **(F)** Arrowheads and asterisk indicate processes of GFAP-positive astrocytes and an amyloid plaque, respectively. Scale bars = **(E)** 100 μm; **(F)** 20 μm. **(G, H)** Hematopoietic prostaglandin D synthase (HPGDS) immunocytochemistry on a Tg2576 mouse brain. HPGDS-positive cells surround a small reactive amyloid plaque **(G)** but not the large burned out class of plaques **(H)**. Asterisks indicate amyloid plaques. Scale bar = 20 μm. **(I)** Double immunofluorescence for HPGDS (pink) and Iba1 (green). Some of the Iba1-positive microglia express HPGDS. Scale bar = 50 μm. Inset shows a high magnification view of double-positive cells showing morphologic characteristics of ameboid microglia. **(J)** Double immunofluorescence for DP_1 (red) and GFAP (green). DP_1 is expressed on the processes of reactive astrocytes that have extended toward the center of this amyloid plaque. Scale bar = 10 μm.

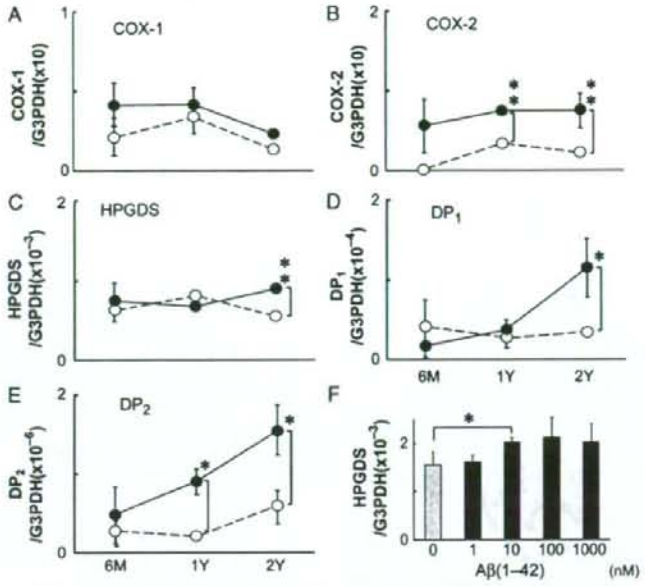

FIGURE 6. (A–E) Number of copies of mRNA for cyclooxygenase (COX)-1, COX-2, hematopoietic prostaglandin D synthase (HPGDS), DP_1, and DP_2 relative to that of glyceraldehyde-3-phosphate dehydrogenase (G3PDH) in brains from Tg2576 mouse (closed circles) and wild-type mouse (open circles) taken at the age of 6 months, 1 year, and 2 years (n = 3). *, $p < 0.05$; **, $p < 0.01$. **(F)** Number of copies of HPGDS mRNA relative to that of G3PDH from primary cultures of microglia before and after amyloid β (Aβ) (1-42) stimulation (n = 3) *, $p < 0.05$.

further increase was observed at concentrations higher than 10 nM (Fig. 6F).

DISCUSSION

HPGDS/PGD_2/DP_1 Signaling Pathway Plays Important Roles in Inflammatory Reactions Within the Senile Plaques

We demonstrated that expression of HPGDS and DP_1 was increased in reactive astrocytes and microglia encircling senile plaques in the AD brain. In contrast, the mRNA levels of all other prostanoid synthases and receptors were almost the same between AD and control groups. A previous study by Iwamoto et al (15) demonstrated that the amounts of PGD_2 and TXB_2 were significantly increased in the brains of Alzheimer-type dementia patients, although other prostaglandin metabolites in their AD group showed no significant changes from normal patients. In this study, we used a more specific and sensitive criterion for AD (9) and determined the levels of prostaglandin synthases and receptors instead of direct prostaglandin determination, because the latter is subject to a large postmortem artifact (16). In addition, we chose the most recent cases with the least postmortem interval for more accurate mRNA analysis. Ages and the postmortem interval of the patients at autopsy were not significantly different between AD and control groups.

Senile plaques have different characteristics depending on their stages (17); for example, there are primitive, neuritic (classic), and burned out class of plaques in various stage of human diseases. α-Macroglobulin and anti-chymotrypsin are expressed in the neuritic-type plaques but not in the burned out ones (18, 19). Although plaques homologous with neuritic plaques were not recognized in Tg2576 mouse brains, we observed that HPGDS expression was limited mainly to the relatively small plaques with surrounding activated microglia and was diminished in the burned out class of plaques in both human and mouse AD brains. These observations may explain why some patients did not show HPGDS mRNA upregulation and may suggest that HPGDS is responsible for early inflammation caused by Aβ accumulation in the evolution of amyloid plaques.

The question as to which is first, plaques or inflammation, still remains to be clarified. We previously demonstrated that secondary demyelination was suppressed by inhibition of PGD_2 production (8). We consider, therefore, that once the plaque is formed, microglia and astrocytes are activated and produce cytokines, which cause further neuronal injury and plaque formation. To clarify this, additional investigation is needed.

New Potential Therapies for Alzheimer Disease Based on Inhibition of the Hematopoietic Prostaglandin D Synthase/Prostaglandin D_2/DP_1 Signaling Pathway

Many epidemiologic and animal studies have revealed that nonsteroidal anti-inflammatory drugs (NSAIDs) are

beneficial for AD patients (20–24). For example, a large, prospective and population-based cohort study confirmed that the relative risk of developing AD was significantly reduced in long-term users of NSAIDs compared with nonusers (25). Furthermore, orally administered ibuprofen produced significant diminution of the ultimate number of amyloid deposits as well as significantly reduced gliosis in Tg2576 mice (24).

PGD_2 is formed from arachidonic acid, which is released from the lipid portion of membranes by $cPLA_2$, by successive enzyme reactions mediated by COX and PGD synthases. COXs, expression of which is upregulated in the AD brain (26, 27), are the major targets of NSAIDs. NSAIDs may reduce the plaque pathology through either their anti-inflammatory actions or suppression of γ-secretase activity (28, 29) or both. The latter reduces the level of the 42-amino acid form of Aβ protein (Aβ42), the most toxic form of the protein. NSAIDs inhibit the constitutively expressed COX-1 as well as the inducible COX-2, both of which produce PGH_2, a common precursor of PGD_2, PGE_2, $PGF_{2\alpha}$, prostacyclin (PGI_2), and TXA_2 (30). PGD_2 is well known as an inflammatory mediator: it augments vascular permeability (31), regulates chemotaxis (32) and antigen presentation (33), and inhibits platelet aggregation (34). The biologic actions of PGD_2 are elicited through binding to its receptors, DP_1 (35) or DP_2 (32). Regarding the anti-inflammatory property of NSAIDs, 3 molecular targets of these drugs have been identified so far in AD: COX-1, COX-2, and PPARγ. NSAIDs not only inhibit the activity of COXs but also activate the nuclear PPARγ (36), which inhibits the production of pro-inflammatory cytokines. All 3 of these NSAID targets seem to be expressed by activated microglia (5). In this study, the level of PPARγ was not changed in AD brains, although this finding does not exclude the possibility of PPARγ-mediated neuroprotection by NSAIDs.

COX-2 has been the major target of anti-inflammatory therapy and a previous study showed an approximately 25% increase in the COX-2 level in the frontal cortex of AD brains (n = 17) compared with that in control brains (n = 12), as determined by densitometric analysis of Northern blots (37). We detected upregulation of COX-2 mRNA in Tg2576 mouse brains but not in the 17 AD frontal cortices by quantitative RT-PCR analysis. Ueno et al (38) reported that HPGDS preferentially utilized COX-1 in the A23187-induced immediate response for PGD_2 synthesis. Therefore, which COX was upregulated along with HPGDS induction needs to be clarified. Although an inflammatory response can have either a potentially beneficial or detrimental outcome, the administration of an HPGDS inhibitor, HQL-79, to the twitcher mouse, which is an animal model of Krabbe disease, remarkably ameliorated their astrogliosis as well as their clinical symptoms (8). HPGDS inhibitors and DP_1 antagonists have already been developed as antiallergic drugs (39), and HQL-79 is an orally active inhibitor of HPGDS (40, 41) that can penetrate through the blood-brain barrier. These drugs will specifically inhibit the PGD_2 signaling pathway, whereas NSAIDs may inhibit the production of all prostanoids, including the neuroprotective PGE_2 (42, 43).

In conclusion, we propose that PGD_2 is a novel inflammatory mediator in the AD brain and that the efficacy of HPGDS inhibitors and DP_1 antagonists should be investigated for halting the devastating course of AD.

ACKNOWLEDGMENTS

We thank Dr. Shinichi Kousaka, National Center of Neurology and Psychiatry, Japan, for the generous gift of the anti-Iba1 antibody. We thank Ms. Shigeko Matsumoto for performing the immunocytochemical analysis and Ms. Megumi Yamaguchi, Ms. Megumi Yamada, and Ms. Taeko Nishimoto for their secretarial assistance.

REFERENCES

1. Selkoe DJ. Alzheimer's disease: Genes, proteins, and therapy. Physiol Rev 2001;81:741–66
2. Griffin WS, Stanley LC, Ling C, et al. Brain interleukin 1 and S-100 immunoreactivity are elevated in Down syndrome and Alzheimer disease. Proc Natl Acad Sci U S A 1989;86:7611–15
3. Rogers J, Luber-Narod J, Styren SD, et al. Expression of immune system-associated antigens by cells of the human central nervous system: Relationship to the pathology of Alzheimer's disease. Neurobiol Aging 1988;9:339–49
4. Pike CJ, Cummings BJ, Cotman CW. Early association of reactive astrocytes with senile plaques in Alzheimer's disease. Exp Neurol 1995; 132:172–79
5. Akiyama H, Barger S, Barnum S, et al. Inflammation and Alzheimer's disease. Neurobiol Aging 2000;21:383–421
6. Hsiao K, Chapman P, Nilsen S, et al. Correlative memory deficits, Aβ elevation, and amyloid plaques in transgenic mice. Science 1996;274: 99–102
7. Kawarabayashi T, Younkin LH, Saido TC, et al. Age-dependent changes in brain, CSF, and plasma amyloid (β) protein in the Tg2576 transgenic mouse model of Alzheimer's disease. J Neurosci 2001;21:372–81
8. Mohri I, Taniike M, Taniguchi H, et al. Prostaglandin D_2-mediated microglia/astrocyte interaction enhances astrogliosis and demyelination in twitcher. J Neurosci 2006;26:4383–93
9. Murayama S, Saitoh Y. Neuropathological diagnostic criteria for Alzheimer disease. Neuropathology 2004;24:254–60
10. Hughes CP, Berg L, Danziger WL, et al. A new clinical scale for the staging of dementia. Br J Psychiatry 1982;140:566–72
11. Lazarus M, Kubata BK, Eguchi N, et al. Biochemical characterization of mouse microsomal prostaglandin E synthase-1 and its colocalization with cyclooxygenase-2 in peritoneal macrophages. Arch Biochem Biophys 2002;397:336–41
12. Mohri I, Eguchi N, Suzuki K, et al. Hematopoietic prostaglandin D synthase is expressed in microglia in the developing postnatal mouse brain. Glia 2003;42:263–74
13. Forman BM, Tontonoz P, Chen J, et al. 15-Deoxy-δ 12,14-prostaglandin J_2 is a ligand for the adipocyte determination factor PPARγ. Cell 1995; 83:803–12
14. Kagitani-Shimono K, Mohri I, Oda H, et al. Lipocalin-type prostaglandin D synthase (β-trace) is upregulated in the αB-crystallin-positive oligodendrocytes and astrocytes in the chronic multiple sclerosis. Neuropathol Appl Neurobiol 2006;32:64–73
15. Iwamoto N, Kobayashi K, Kosaka K. The formation of prostaglandins in the postmortem cerebral cortex of Alzheimer-type dementia patients. J Neurol 1989;236:80–84
16. Narumiya S, Ogorochi T, Nakao K, et al. Prostaglandin D_2 in rat brain, spinal cord and pituitary: Basal level and regional distribution. Life Sci 1982;31:2093–2103
17. Probst A, Brunnschweiler H, Lautenschlager C, et al. A special type of senile plaque, possibly an initial stage. Acta Neuropathol (Berl) 1987; 74:133–41
18. Van Gool D, De Strooper B, Van Leuven F, et al. α_2-Macroglobulin expression in neuritic-type plaques in patients with Alzheimer's disease. Neurobiol Aging 1993;14:233–37

19. Van Gool D, Carmeliet G, Triau E, et al. Appearance of localized immunoreactivity for the α4 integrin subunit and for fibronectin in brains from Alzheimer's, Lewy body dementia patients and aged controls. Neurosci Lett 1994;170:71–73
20. Jenkinson ML, Bliss MR, Brain AT, et al. Rheumatoid arthritis and senile dementia of the Alzheimer's type. Br J Rheumatol 1989;28:86–88
21. Rogers J, Kirby LC, Hempelman SR, et al. Clinical trial of indomethacin in Alzheimer's disease. Neurology 1993;43:1609–11
22. Rich JB, Rasmusson DX, Folstein MF, et al. Nonsteroidal anti-inflammatory drugs in Alzheimer's disease. Neurology 1995;45:51–55
23. McGeer PL, Schulzer M, McGeer EG. Arthritis and anti-inflammatory agents as possible protective factors for Alzheimer's disease: A review of 17 epidemiologic studies. Neurology 1996;47:425–32
24. Lim GP, Yang F, Chu T, et al. Ibuprofen suppresses plaque pathology and inflammation in a mouse model for Alzheimer's disease. J Neurosci 2000;20:5709–14
25. in t' Veld BA, Ruitenberg A, Hofman A, et al. Nonsteroidal anti-inflammatory drugs and the risk of Alzheimer's disease. N Engl J Med 2001;345:1515–21
26. Fiala M, Liu QN, Sayre J, et al. Cyclooxygenase-2-positive macrophages infiltrate the Alzheimer's disease brain and damage the blood-brain barrier. Eur J Clin Invest 2002;32:360–71
27. Hoozemans JJ, Bruckner MK, Rozemuller AJ, et al. Cyclin D1 and cyclin E are co-localized with cyclo-oxygenase 2 (COX-2) in pyramidal neurons in Alzheimer disease temporal cortex. J Neuropathol Exp Neurol 2002;61;678–88
28. Eriksen JL, Sagi SA, Smith TE, et al. NSAIDs and enantiomers of flurbiprofen target gamma-secretase and lower Aβ42 in vivo. J Clin Invest 2003;112:440–49
29. Weggen S, Eriksen JL, Sagi SA, et al. Aβ42-lowering nonsteroidal anti-inflammatory drugs preserve intramembrane cleavage of the amyloid precursor protein (APP) and ErbB-4 receptor and signaling through the APP intracellular domain. J Biol Chem 2003;278:30748–54
30. Smith WL, DeWitt DL, Garavito RM. Cyclooxygenases: Structural, cellular, and molecular biology. Annu Rev Biochem 2000;69:145–82
31. Flower RJ, Harvey EA, Kingston WP. Inflammatory effects of prostaglandin D_2 in rat and human skin. Br J Pharmacol 1976;56:229–33
32. Hirai H, Tanaka K, Yoshie O, et al. Prostaglandin D_2 selectively induces chemotaxis in T helper type 2 cells, eosinophils, and basophils via seven-transmembrane receptor CRTH2. J Exp Med 2001;193:255–61
33. Herve M, Angeli V, Pinzar E, et al. Pivotal roles of the parasite PGD_2 synthase and of the host D prostanoid receptor 1 in schistosome immune evasion. Eur J Immunol 2003;33:2764–72
34. Whittle BJ, Moncada S, Vane JR. Comparison of the effects of prostacyclin (PGI_2), prostaglandin E_1 and D_2 on platelet aggregation in different species. Prostaglandins 1978;16:373–88
35. Hirata M, Kakizuka A, Aizawa M, et al. Molecular characterization of a mouse prostaglandin D receptor and functional expression of the cloned gene. Proc Natl Acad Sci U S A 1994;91:11192–96
36. Lehmann JM, Lenhard JM, Oliver BB, et al. Peroxisome proliferator-activated receptors α and γ are activated by indomethacin and other non-steroidal anti-inflammatory drugs. J Biol Chem 1997;272:3406–10
37. Pasinetti GM, Aisen PS. Cyclooxygenase-2 expression is increased in frontal cortex of Alzheimer's disease brain. Neuroscience 1998;87:319–24
38. Ueno N, Murakami M, Tanioka T, et al. Coupling between cyclooxygenase, terminal prostanoid synthase, and phospholipase A_2. J Biol Chem 2001;276:34918–27
39. Matsuoka T, Hirata M, Tanaka H, et al. Prostaglandin D_2 as a mediator of allergic asthma. Science 2000;287:2013–17
40. Matsushita N, Aritake K, Takada A, et al. Pharmacological studies on the novel antiallergic drug HQL-79: II. Elucidation of mechanisms for antiallergic and antiasthmatic effects. Jpn J Pharmacol 1998;78:11–22
41. Aritake K, Kado Y, Inoue T, et al. Structural and functional characterization of HQL-79, an orally active, selective inhibitor for human hematopoietic prostaglandin D synthase. J Biol Chem 2006;281:15277–86
42. McCullough L, Wu L, Haughey N, et al. Neuroprotective function of the PGE_2 EP2 receptor in cerebral ischemia. J Neurosci 2004;24:257–68
43. Bilak M, Wu L, Wang Q, et al. PGE_2 receptors rescue motor neurons in a model of amyotrophic lateral sclerosis. Ann Neurol 2004;56:240–48

Lipocalin-type prostaglandin D synthase/β-trace is a major amyloid β-chaperone in human cerebrospinal fluid

Takahisa Kanekiyo*†, Tadato Ban‡, Kosuke Aritake*, Zhi-Li Huang*§, Wei-Min Qu*, Issay Okazaki*, Ikuko Mohri*¶, Shigeo Murayama‖, Keiichi Ozono†, Masako Taniike¶, Yuji Goto‡, and Yoshihiro Urade*,**

*Department of Molecular Behavioral Biology, Osaka Bioscience Institute, Suita, Osaka 565-0874, Japan; †Department of Pediatrics and ¶Mental Health and Environmental Effects Research, The Research Center for Child Mental Development, Graduate School of Medicine, and ‡Institute for Protein Research, Osaka University and CREST Japan Science and Technology Agency, Suita, Osaka 565-0871, Japan; §State Key Laboratory of Medical Neurobiology, Shanghai Medical College of Fudan University, Shanghai 200032, China; and ‖Department of Neuropathology, Tokyo Metropolitan Institute of Gerontology, Itabashi-ku, Tokyo 173-0015, Japan

Communicated by Osamu Hayaishi, Osaka Bioscience Institute, Osaka, Japan, February 21, 2007 (received for review December 25, 2006)

The conformational change in amyloid β (Aβ) peptide from its monomeric form to aggregates is crucial in the pathogenesis of Alzheimer's disease (AD). In the healthy brain, some unidentified chaperones appear to prevent the aggregation of Aβ. Here we reported that lipocalin-type prostaglandin D synthase (L-PGDS)/β-trace, the most abundant cerebrospinal fluid (CSF) protein produced in the brain, was localized in amyloid plaques in both AD patients and AD-model Tg2576 mice. Surface plasmon resonance analysis revealed that L-PGDS/β-trace tightly bound to Aβ monomers and fibrils with high affinity (K_D = 18–50 nM) and that L-PGDS/β-trace recognized residues 25–28 in Aβ, which is the key region for its conformational change to a β-sheet structure. The results of a thioflavin T fluorescence assay to monitor Aβ aggregation disclosed that L-PGDS/β-trace inhibited the spontaneous aggregation of Aβ (1–40) and Aβ (1–42) within its physiological range (1–5 μM) in CSF. L-PGDS/β-trace also prevented the seed-dependent aggregation of 50 μM Aβ with K_i of 0.75 μM. Moreover, the inhibitory activity toward Aβ (1–40) aggregation in human CSF was decreased by 60% when L-PGDS/β-trace was removed from the CSF by immunoaffinity chromatography. The deposition of Aβ after intraventricular infusion of Aβ (1–42) was 3.5-fold higher in L-PGDS-deficient mice and reduced to 23% in L-PGDS-overexpressing mice as compared with their wild-type levels. These data indicate that L-PGDS/β-trace is a major endogenous Aβ-chaperone in the brain and suggest that the disturbance of this function may be involved in the onset and progression of AD. Our findings may provide a diagnostic and therapeutic approach for AD.

aggregation | Alzheimer's disease | mouse | surface plasmon resonance | thioflavin T

The conformational change in amyloid β (Aβ) peptides, Aβ (1–40) and Aβ (1–42), from their soluble monomeric forms to insoluble aggregates is central to the pathogenesis of Alzheimer's disease (AD). Aβ (1–42) peptide is probably the pathogenic one in AD (1–3). Mutations in either amyloid precursor protein or presenilin 1 and 2 genes result in Aβ overproduction (1–3) and have been detected in early onset familial cases of AD, which account for ≈3% of AD patients (4, 5). In contrast, Aβ production in late-onset sporadic cases of AD, which represent the majority of AD cases, remains unchanged, yet the aggregation of Aβ is enhanced. Functional abnormalities in the deterrents against Aβ aggregation would seem, therefore, to be involved in the pathogenesis of sporadic AD. Aβ is secreted into human cerebrospinal fluid (CSF) under normal conditions (6), and in the healthy brain, it appears to be efficiently controlled by some unidentified extracellular chaperones so as not to aggregate. In the present study, we focused on the possibility of lipocalin-type prostaglandin D synthase (L-PGDS) (7, 8), a major human CSF protein known as β-trace (9), being such a chaperone that functions to prevent Aβ misfolding and aggregation.

Results

Immunostaining of L-PGDS/β-Trace in Amyloid Plaques. When we immunostained for L-PGDS/β-trace in the brain of 2-year-old male AD model Tg2576 mice, L-PGDS/β-trace was detected in many amyloid plaques (Fig. 1 *A*, arrowheads, and *B*, asterisk), as well as in the leptomeninges (Fig. 1*A*, small double arrow) as described previously (10, 11). The L-PGDS/β-trace immunoreactivity was not observed in amyloid plaques when preabsorbed antibody was used (Fig. 1*C*). Double immunofluorescence staining with anti-Aβ antibody (Fig. 1*D*) and anti-L-PGDS/β-trace antibody (Fig. 1*E*) also revealed that L-PGDS/β-trace was localized in Aβ-positive amyloid plaques (Fig. 1*F*, asterisks). In the brain of a late-onset sporadic AD patient, we also confirmed that L-PGDS/β-trace was immunohistochemically detectable in senile plaques in the frontal cortex (Fig. 1*G*, arrowheads, and *H*, asterisk). These data suggest that L-PGDS/β-trace may bind to Aβ fibrils.

Binding of L-PGDS/β-Trace to Aβ Peptides. To investigate the binding of L-PGDS/β-trace to Aβ peptides, we monitored the changes in molecular mass of Aβ (1–40) immobilized on a sensor chip after infusion of various concentrations of L-PGDS/β-trace solution on the chip by surface plasmon resonance (SPR) analysis. L-PGDS/β-trace purified from human CSF rapidly bound to the immobilized Aβ (1–40) in a dose-dependent manner and thereafter very slowly dissociated from it after washing with 50 mM sodium phosphate (pH 7.5) and 100 mM NaCl. According to the association and dissociation kinetics, the dissociation constant (K_D) value for the binding affinity was calculated to be 50 nM (Fig. 2*A*). Conversely, Aβ (1–40) monomer also bound to the immobilized L-PGDS/β-trace with a similar high affinity at the K_D value of 60 nM (Fig. 2*B*). L-PGDS/β-trace also bound to immobilized Aβ (1–42), Aβ (1–40) fibrils, and Aβ (1–42) fibrils with high affinities (K_D = 40–43 nM; Table 1).

To address which regions of Aβ were involved in the binding to L-PGDS/β-trace, we used several segments of Aβ peptides for SPR analysis. L-PGDS/β-trace tightly bound to Aβ (25–35) and

Author contributions: T.K., Y.G., and Y.U. designed research; T.K., T.B., K.A., Z.-L.H., W.-M.Q., and I.O. performed research; T.K., Z.-L.H., W.-M.Q., I.M., S.M., K.O., M.T., Y.G., and Y.U. analyzed data; and T.K., Z.-L.H., and Y.U. wrote the paper.

The authors declare no conflict of interest.

Abbreviations: Aβ, amyloid β; AD, Alzheimer's disease; AFM, atomic force microscopy; CSF, cerebrospinal fluid; L-PGDS, lipocalin-type prostaglandin D synthase; SPR, surface plasmon resonance; ThT, thioflavin T.

**To whom correspondence should be addressed. E-mail: uradey@obi.or.jp.

This article contains supporting information online at www.pnas.org/cgi/content/full/0701585104/DC1.

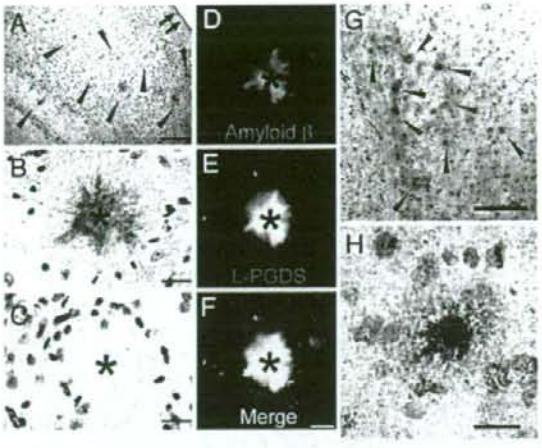

Fig. 1. L-PGDS/β-trace immunostaining of amyloid plaques in Tg2576 mice and AD patients. (*A–F*) Amyloid plaques in the cerebral cortex of Tg2576 mice (*A*, arrowheads; *B* and *C*, asterisk) were immunopositive with anti-mouse L-PGDS/β-trace antibody (*A* and *B*), but not with preabsorbed antibody (*C*). Double immunofluorescence staining of Aβ (*D*) and L-PGDS/β-trace (*E*) showed that they were colocalized (*F*, merged image). (*G* and *H*) In the frontal cortex of a 70-year-old AD patient, amyloid plaques (*G*, arrowheads; *H*, asterisk) were immunostained by anti-human L-PGDS/β-trace polyclonal antibody. (Scale bars: *A* and *G*, 200 μm; *B–F* and *H*, 20 μm.)

Aβ (1–28) peptides with K_D values of 20 and 40 nM, respectively, but not to Aβ (1–16) (Table 1), thus indicating that L-PGDS/β-trace recognized residues 25–28 of Aβ. Recombinant human L-PGDS expressed in *Eschericha coli* also tightly bound to Aβ peptides with K_D values of 18–31 nM.

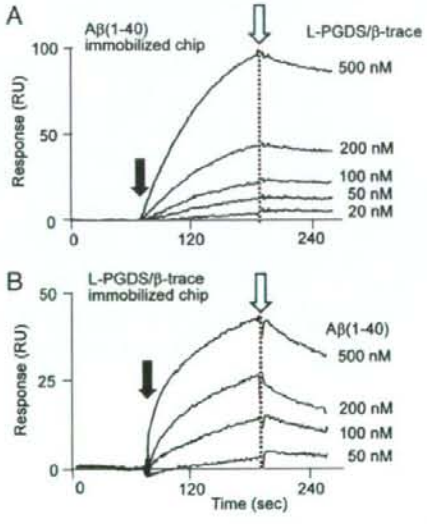

Fig. 2. SPR analysis of binding between L-PGDS/β-trace and Aβ. (*A*) Binding of L-PGDS/β-trace to 2 ng of immobilized Aβ (1–40). (*B*) Binding of Aβ (1–40) to 8 ng of immobilized Aβ L-PGDS/β-trace. Filled and open arrows show the starting points for sample injection and washing with buffer, respectively. Human serum albumin did not bind to Aβ (1–40) in the same concentration range.

Table 1. K_D values of L-PGDS/β-trace and recombinant L-PGDS to various Aβ peptides by SPR analysis

	K_D, nM	
Peptides	L-PGDS/β-trace	Recombinant human L-PGDS
Aβ (1–40)	50	20
Aβ (1–42)	43	27
Aβ (1–40) fibril	42	31
Aβ (1–42) fibril	40	26
Aβ (25–35)	20	18
Aβ (1–28)	40	19
Aβ (1–16)	Not detected	Not detected

L-PGDS/β-trace purified from human CSF or recombinant human L-PGDS was applied to the various immobilized Aβ peptides. According to the association and dissociation curves, K_D values for the binding affinity were calculated.

Inhibition of Aβ Aggregation by L-PGDS/β-Trace *in Vitro*. Next, we investigated the effect of L-PGDS/β-trace on spontaneous Aβ aggregation *in vitro* (Fig. 3). The results of a thioflavin T (ThT) fluorescence assay to monitor Aβ aggregation revealed that the fibrillogenesis phase of 50 μM Aβ (1–40) aggregation commenced 24 h subsequent to initiation of the nucleation phase and reached a plateau 48 h thereafter. L-PGDS/β-trace at 1 μM extended the nucleation phase and decreased the final amount of Aβ aggregates to 49% of that in its absence. L-PGDS/β-trace at 5 μM inhibited all spontaneous Aβ aggregation for at least 168 h (Fig. 3*A*). The fibrillogenesis of Aβ (1–42) commenced even earlier, 6 h after the nucleation phase had begun, and Aβ aggregation reached a plateau within 24 h. L-PGDS/β-trace at 1 μM extended the nucleation phase and decreased the final amount of Aβ aggregates to 62% of that in its absence. The aggregation of Aβ (1–42) was also completely inhibited for at least 168 h in the presence of 5 μM L-PGDS/β-trace (Fig. 3*B*). The aggregation of both Aβ (1–40) and Aβ (1–42) was prevented in a dose-dependent manner by the addition of either 1 or 5 μM L-PGDS/β-trace, and concentrations are in the physiological range in human CSF (12).

When Aβ fibrils were added as a "seed," the fibrillogenesis was remarkably accelerated. This seed-dependent aggregation of Aβ was also inhibited by L-PGDS/β-trace [Fig. 3 *C* and *D* and supporting information (SI) Fig. 7*A*]. Albumin is the most abundant human CSF protein with the physiological range ≈2–8 μM in human CSF (13). Albumin partially inhibited Aβ aggregation, yet did not completely prevent the seed-dependent aggregation of 50 μM Aβ (1–40) within its physiological range (SI Fig. 7*B*). Total internal reflection fluorescence microscopy revealed that large Aβ fibrils were produced after incubation of 50 μM Aβ (1–40) monomer with the seed (Fig. 3*C Left*); however, such fibrils were not observed in the presence of 5 μM L-PGDS/β-trace (Fig. 3*C Right*). The inhibitory effect of L-PGDS/β-trace on Aβ fibrillogenesis was confirmed by inspection by atomic force microscopy (AFM) (Fig. 3*D*).

As revealed by circular dichroism (CD) spectrum analysis, the Aβ monomer possessed a predominantly unfolded conformation (Fig. 3*E*, black). When the Aβ monomer was incubated with a seed, a CD spectrum with a minimum at ≈220 nm appeared, indicating the formation of amyloid fibrils with the β-sheet structure (14) (Fig. 3*E*, blue). However, in the presence of L-PGDS/β-trace, Aβ did not assume the β-sheet-rich structure (Fig. 3*E*, red), indicating that L-PGDS/β-trace prevented the conformational change to the β-sheet structure. These results are consistent with the results of the ThT fluorescence assay described above.

The rate of fibrillogenesis of the seed-dependent Aβ (1–40) aggregation was decreased in a concentration-dependent man-

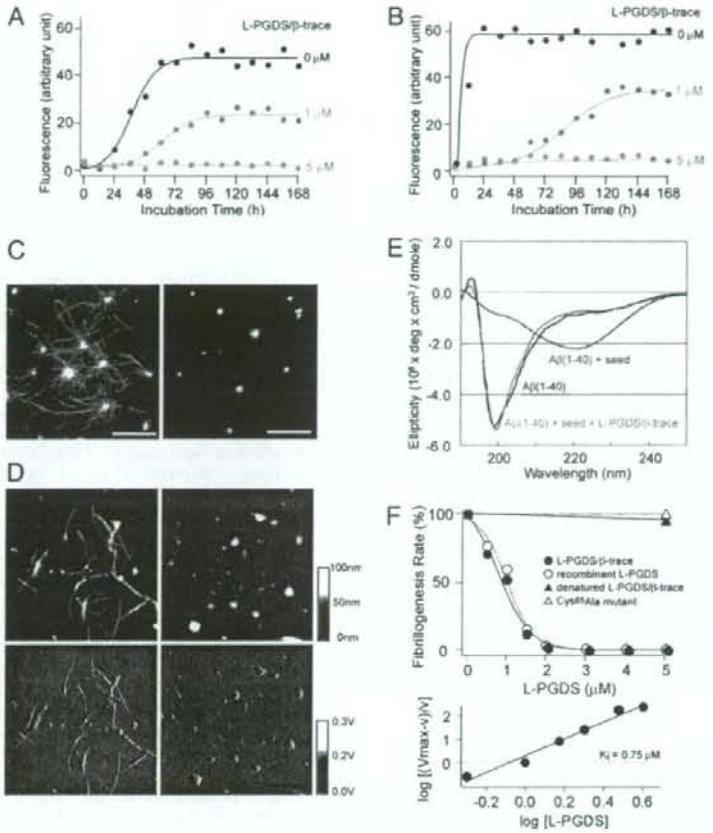

Fig. 3. Inhibition of Aβ aggregation by L-PGDS/β-trace. (*A* and *B*) Spontaneous aggregation of 50 μM Aβ (1–40) (*A*) and Aβ (1–42) (*B*) in the absence (black) or presence of L-PGDS/β-trace (orange, 1 μM; green, 5 μM). (*C* and *D*) Observations of Aβ (1–40) seed-dependent aggregation by fluorescence abscence (black) or microscopy (*C*) and AFM (*D*) in the absence (*Left*) or presence (*Right*) of L-PGDS/β-trace. (Scale bars: *C*, 10 μm; *D*, 1 μm.) (*E*) CD spectra of 50 μM Aβ (1–40) before (black) and after incubation for 2 h with Aβ seed (10 μg/ml) in the absence (blue) or presence of 5 μM L-PGDS/β-trace (red). (*F Upper*) Inhibition of seed-dependent fibrillogenesis of 50 μM Aβ (1–40) by incubation for 1 h with L-PGDS/β-trace purified from human CSF (closed circles), recombinant human L-PGDS (open circles), heat-denatured L-PGDS/β-trace (closed triangles), or recombinant inactive Cys^{65}Ala mutant of human L-PGDS (open triangles). (*F Lower*) Hill plot of the data obtained for L-PGDS/β-trace purified from human CSF.

ner by either L-PGDS/β-trace purified from human CSF or the recombinant L-PGDS (Fig. 3*F Upper*). The kinetic inhibitory constant (K_i) of L-PGDS/β-trace with respect to Aβ (1–40) aggregation was calculated by Hill plot analysis to be 0.75 μM (Fig. 3*F Lower*). The inhibitory activity against the Aβ (1–40) aggregation was observed with neither heat-denatured L-PGDS/β-trace nor a recombinant inactive Cys^{65}Ala mutant of human L-PGDS (the catalytically active Cys^{65} residue was replaced; Fig. 3*F Upper*). These results indicate that L-PGDS/β-trace has a specific conformation required for its interaction with Aβ, and that the Cys^{65} residue is crucial for the chaperone activity of L-PGDS/β-trace to prevent Aβ aggregation.

Preventive Effect of L-PGDS/β-Trace in Human CSF on Aβ Aggregation. L-PGDS/β-trace could be almost completely removed from human CSF by passage through a mouse monoclonal anti-L-PGDS/β-trace antibody-conjugated column (Fig. 4*A*). When we compared the inhibitory effect of human CSF and L-PGDS/β-trace-free CSF on Aβ aggregation, 50% human CSF prevented spontaneous aggregation of Aβ (1–40) for 96 h and 50% L-PGDS/β-trace-free CSF for 48 h (Fig. 4*B*). After incubation for 96 h, human CSF and L-PGDS/β-trace-free CSF prevented 90% and 36%, respectively, of the spontaneous aggregation of Aβ (1–40), indicating that L-PGDS/β-trace was the major CSF component responsible for the inhibition of Aβ aggregation (Fig. 4*C*).

Inhibition of Aβ Deposition by L-PGDS/β-Trace *in Vivo*. To test whether L-PGDS/β-trace could prevent Aβ aggregation *in vivo*, we injected biotin-labeled human Aβ (1–42) into the lateral ventricle of the brain of WT, L-PGDS-knockout (L-PGDS$^{-/-}$; C57BL/6 strain), and human L-PGDS-transgenic (L-PGDS-Tg; FVB strain) mice. As examined by avidin–biotin–peroxidase staining, deposits of biotin-labeled Aβ (1–42) were detected along the lateral ventricle at 3 h postinjection in all sections examined (Fig. 5). As compared with WT mice (Fig. 5 *A*, *C*, *E*, and *G*), Aβ (1–42) deposition was histologically accelerated in L-PGDS$^{-/-}$ mice (Fig. 5 *B* and *F*) and reduced in L-PGDS-Tg mice (Fig. 5 *D* and *H*). Moreover, Aβ deposits were positively stained by Congo-red staining (Fig. 5 *I–L*), indicating that the deposits were composed of Aβ fibrils rather than Aβ monomers.

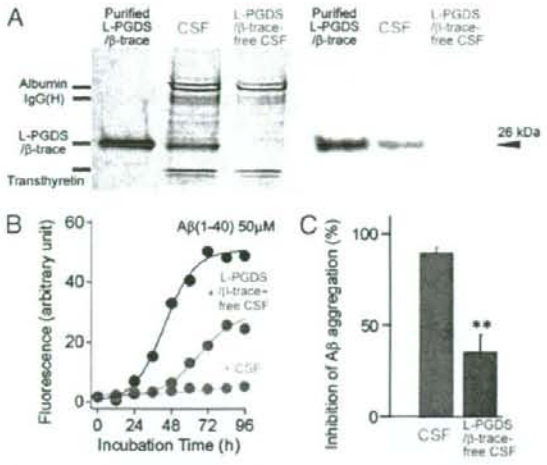

Fig. 4. Inhibitory effect of L-PGDS/β-trace in human CSF on Aβ aggregation. (*A*) SDS/PAGE and Western blot analysis revealed that L-PGDS/β-trace is a major protein in human CSF with a molecular mass of 26 kDa and is almost completely removed from the CSF by passage through a mouse monoclonal anti-L-PGDS antibody-conjugated column. (*B*) Representative time course of the spontaneous Aβ aggregation in the absence (black) or presence of 50% human CSF (red) or 50% L-PGDS/β-trace-free CSF (blue). (*C*) Inhibition of Aβ aggregation in the presence of 50% CSF or the L-PGDS/β-trace-free CSF. The percentage inhibition of Aβ aggregation was calculated by using the formula $[1 - (Fa/Fb)] \times 100$, where *Fb* and *Fa* are the ThT fluorescence intensities of 50 μM Aβ (1–40) incubated for 96 h or in the presence of 50% CSF or L-PGDS/β-trace-free CSF, respectively. Data are expressed as the mean ± SEM of three independent experiments. **, $P < 0.01$ vs. CSF (Student's *t* test).

Next deposition of Aβ (1–42) was quantified by binding of [^{125}I]-streptavidin to brain sections prepared from L-PGDS$^{-/-}$ (7BL/6 strain; Fig. 5*M*) and L-PGDS-Tg (Fig. 5*N*) mice and their WT counterparts, and sections had been immunostained with biotin-labeled Aβ (1–42). The deposition of Aβ (1–42) was 3.5-fold higher in L-PGDS$^{-/-}$ mice than in WT mice (Fig. 5*M*) and 77% lower in L-PGDS-Tg mice than in WT mice (Fig. 5*N*). These results clearly indicate that L-PGDS/β-trace strongly inhibited Aβ aggregation and deposition *in vivo*.

Discussion

In this study, we demonstrated that L-PGDS/β-trace plays a critical role as an endogenous Aβ-chaperone, thereby inhibiting both Aβ (1–40) and Aβ (1–42) aggregation *in vitro* and *in vivo*. SPR analysis showed that L-PGDS/β-trace tightly bound to Aβ (1–28) and Aβ (25–35), but not to Aβ (1–16), indicating that the hydrophobic region from residues 25–28 of Aβ was crucial for the binding to L-PGDS/β-trace. Interestingly, these same residues in Aβ are the key region for the conformational change in Aβ peptides from the random-coiled to the β-sheet structure (15). During Aβ aggregation, soluble Aβ peptides are known to change their conformation to the β-sheet structure and aggregate to form insoluble fibrils enriched in β-sheet structure (15, 16). The interaction of L-PGDS/β-trace with residues 25–28 in Aβ may prevent this conformational change to the β-sheet structure (Fig. 6), as was suggested by far-UV CD spectrum analysis (Fig. 3*E*). L-PGDS/β-trace completely prevented Aβ aggregation even at a molar ratio of 1:10. These results suggest that L-PGDS/β-trace catalyzes this conformational change in Aβ from the β-sheet to the random-coiled structure.

The aggregation of Aβ was earlier shown to be inhibited by apolipoprotein (Apo) E (17, 18) and transthyretin (19). Because of the disturbance of Aβ metabolism (17, 18), ApoE is a risk factor for late-onset AD. The ε4 allele of ApoE shows an incidence of 17.5% among all AD cases (4, 5). However, ApoE is not a CNS-specific protein (13, 20), whereas Aβ is primarily produced in the brain (6, 7). On the other hand, L-PGDS/β-trace is the most abundant CSF protein produced in the brain and is dominantly expressed in the CNS rather than in the peripheral organs. L-PGDS/β-trace exists more abundantly in the brain than ApoE. Furthermore, L-PGDS/β-trace binds to Aβ with an affinity (K_D = 18–50 nM) comparable with that of ApoE (K_D = 20 nM) (21). Therefore, L-PGDS/β-trace could be considered more essential than ApoE for the prevention of Aβ aggregation in the brain.

Based on these findings, the incidence of Aβ aggregation would be expected to increase when the L-PGDS/β-trace concentration is decreased or the Aβ-chaperone activity of L-PGDS/β-trace is inactivated in the brain. Two-dimensional gel electrophoresis analysis (22) revealed that L-PGDS/β-trace is decreased in CSF of AD patients as compared with control healthy individuals. In postmenopausal depression, a known risk factor for AD (23), the decrease in the estradiol level is known to elicit a decrease in L-PGDS/β-trace expression (24). In addition, a polymorphism in L-PGDS/β-trace with a C-terminal exon 6-truncation was found in AD patients and claimed to be another risk factor for AD (38). Because C-terminal deletion results in the unfolding and inactivation of L-PGDS/β-trace (25), such mutation is predicted to decrease L-PGDS/β-trace chaperone activity. Moreover, the CSF levels of small hydrophobic molecules such as bilirubin and biliverdin, which bind to L-PGDS/β-trace (26), have been reported to be increased in AD patients (27) and inactivate the Aβ-chaperone activity of L-PGDS/β-trace (T.K., unpublished results). It is reasonable, therefore, to posit that functional disturbances of L-PGDS/β-trace may lead to the sporadic late-onset cases of AD.

Quantitative and qualitative changes in the Aβ-chaperone activity of L-PGDS/β-trace, therefore, may serve as biomarkers for predicting the onset of AD. Further, as the high-resolution x-ray crystallographic structure of L-PGDS has already been determined, it may be possible to design recombinant L-PGDS with a higher affinity for Aβ or to develop novel drugs to increase the affinity of L-PGDS/β-trace for Aβ for use in the therapy of AD. Interestingly, environmental enrichment, as compared with standard animal housing conditions, increased L-PGDS/β-trace gene expression and reduced Aβ deposition in the brain of amyloid precursor protein transgenic mice (28), indicating that the up-regulation of L-PGDS/β-trace may suppress Aβ deposition. That report is in good agreement with our conclusion that L-PGDS/β-trace is the major endogenous Aβ-chaperone to prevent Aβ aggregation in the brain. Our findings thus provide a new insight into the molecular mechanism of AD pathogenesis and a potential therapeutic strategy for AD.

Materials and Methods

Animals. Tg2576 mice (29) were purchased from The Jackson Laboratory (Bar Harbor, ME). L-PGDS$^{-/-}$ mice (30, 31) and human L-PGDS-Tg mice (B20) (32) were generated at the Osaka Bioscience Institute (Osaka, Japan). The experimental protocols employing mice were approved by the Animal Care Committee of Osaka Bioscience Institute, and every effort was made to minimize the number of animals used as well as any pain and discomfort.

Autopsy Brain Tissues. Brain tissues from pathologically diagnosed AD patients were obtained from the Brain Bank of Tokyo Metropolitan Geriatric Hospital and Tokyo Metropolitan Institute of Gerontology (Tokyo, Japan). This study was approved by the institutional review boards of Osaka Bioscience Institute, Tokyo Metropolitan Geriatric Hospital, Tokyo Metropolitan

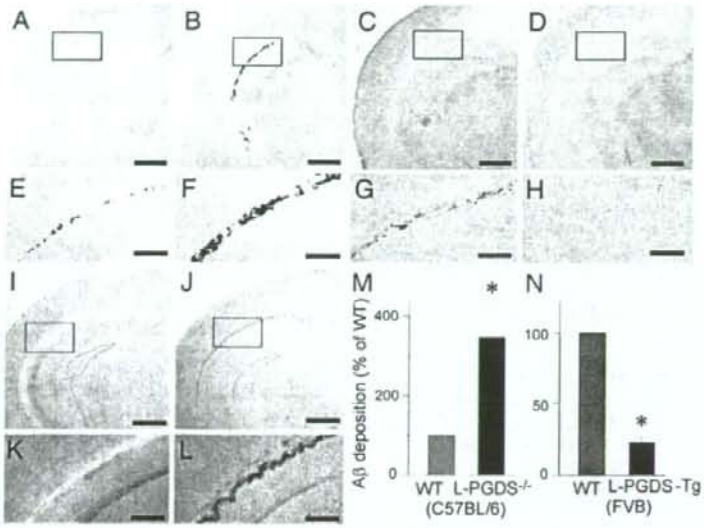

Fig. 5. Inhibition of Aβ deposition by L-PGDS/β-trace *in vivo*. (*A–H*) Aβ deposition in the brain of WT mice (C57BL/6; *A* and *E*), L-PGDS$^{-/-}$ mice (C57BL/6; *B* and *F*), WT mice (FVB; *C* and *G*), and L-PGDS-Tg mice (FVB; *D* and *H*). (Scale bars: *A–D*, 1 mm; *E–H*, 200 μm.) (*I–L*) Congo-red staining of Aβ deposition in WT (C57BL/6; *I* and *K*) and L-PGDS$^{-/-}$ mice (C57BL/6; *J* and *L*) brain as described above. (Scale bar: *I* and *J*, 1 mm; *K* and *L*, 200 μm.) (*M* and *N*) The Aβ deposition was quantified by binding of [^{125}I]-streptavidin to tissue sections prepared from the brain of WT and L-PGDS$^{-/-}$ mice (C57BL/6; *M*) and of WT and L-PGDS-Tg mice (FVB; *N*), which sections had been reacted with biotin-labeled Aβ (1–42). Data are expressed as the mean ± SEM (n = 3–4). Significant difference was based on Student's t test; *, $P < 0.05$.

Institute of Gerontology, and Osaka University Graduate School of Medicine.

Antibodies. Rabbit polyclonal anti-human L-PGDS (1:1,000 dilution) and anti-mouse L-PGDS (1:4,000 dilution) antisera were raised and purified at the Osaka Bioscience Institute. Monoclonal anti-human Aβ (11–28) antibody (1:100; IBL, Gunma, Japan) was also used.

Immunohistochemistry. Deparaffinized sections were preincubated with 0.3% H_2O_2 in methanol followed by 50 mM sodium phosphate (pH 7.5) and 100 mM NaCl containing 0.2% Triton X-100. After pretreatment with formic acid for 5 min and trypsin for 15 min, they were sequentially incubated with primary antibody, biotinylated secondary antibody (Vector Laboratories, Burlingame, CA), and avidin–biotin complex (2 μg/ml; Vector Laboratories) by using the ABC elite kit according to the manufacturer's protocol. Immunoreactivity was visualized with diaminobenzidine (DAB; Dotite, Kumamoto, Japan) solution. For double immunostaining, deparaffinized sections were incubated at 4°C overnight with anti-Aβ and anti-L-PGDS antibody, followed by FITC-conjugated anti-mouse IgG (Vector Laboratories) and Texas Red-conjugated anti-rabbit IgG (ICN Biomedicals, Costa Mesa, CA) for 2 h at room temperature.

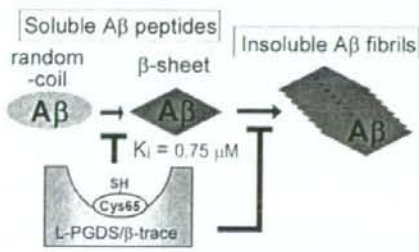

Fig. 6. Proposed schema for inhibition of Aβ aggregation by L-PGDS/β-trace. Soluble Aβ monomers change their conformation from a random-coil dominant structure to the β-sheet-rich structure and then aggregate to insoluble fibrils. L-PGDS/β-trace can prevent Aβ aggregation by inhibiting the transformation of Aβ monomers to β-sheet-rich structure and the sequential seed-dependent Aβ fibrillogenesis.

Preparation of Aβ Solutions. Aβ (1–16), Aβ (25–35), Aβ (1–40), Aβ (1–42) (Peptide Institute, Osaka, Japan), and Aβ (1–28) (AnaSpec, San Jose, CA) were dissolved in 0.02% ammonia solution at 200 μM. The Aβ fibril seed solution was prepared by incubation of 50 μM Aβ peptides in 50 mM sodium phosphate (pH 7.5) and 100 mM NaCl for 7 days at 37°C.

Purification of Human L-PGDS/β-Trace in CSF. Human CSF samples were obtained from the Department of Neurosurgery, Nagoya City University Hospital. Informed consent was obtained from all patients for use of their CSF, sampled by lumbar puncture as part of a diagnostic workup. Human L-PGDS/β-trace was purified from the CSF by immunoaffinity chromatography with a monoclonal anti-human L-PGDS/β-trace antibody 6F5-conjugated column as reported previously (33).

SPR Analysis. The SPR experiments were performed with a BIAcore 2000 (BIAcore AB, Uppsala, Sweden). Aβ monomers, fibrils or L-PGDS/β-trace were immobilized by amine coupling onto a CM5 chip (BIAcore AB) that had been preactivated with a mixture of *N*-ethyl-*N'*-(3-dymethylaminopropyl)carbodimide hydrochloride and *N*-hydroxysuccinimide. After blocking of the remaining activated carboxyl groups on the sensor chip with ethanolamine, the analyte was applied at a flow rate of 20 μl/min in 50 mM sodium phosphate (pH 7.5) and 100 mM NaCl at 25°C. Following measurement, the chip surface was regenerated with

50 mM NaOH. The reference cell was prepared by amine coupling without the ligand.

Fluorescence Spectroscopy. Aβ peptides (50 μM) were incubated at 37°C in the absence or presence of human L-PGDS/β-trace purified from human CSF (34), recombinant human L-PGDS expressed in *E. coli* (35), or human CSF in 50 mM sodium phosphate (pH 7.5) and 100 mM NaCl. The seed-dependent and spontaneous Aβ aggregations were monitored with or without addition of Aβ seed (final concentration 10 μg/ml) in a Hitachi F-4500 fluorescence spectrophotometer (Hitachi Software Engineering, Yokohama, Japan) at excitation and emission wavelengths of 446 and 490 nm, respectively, after the components had been mixed with a 200-fold volume of 50 mM glycine-NaOH (pH 8.5) containing 5 μM ThT (Wako Pure Chemicals, Osaka, Japan) as described earlier (36).

Fluorescence Microscopy and AFM. Aβ (1–40; 50 μM) was incubated for 2 h with the Aβ seed (10 μg/ml) in 50 mM sodium phosphate (pH 7.5) and 100 mM NaCl in the absence or presence of 5 μM L-PGDS/β-trace. The solution was then diluted 5-fold and incubated with ThT of a final concentration of 5 μM. The fibril formation of Aβ on glass slides was examined by fluorescence microscopy (37). In the case of AFM, 10 μl of Aβ solution was spotted on freshly cleaved mica surfaces and left undisturbed for 2 min, after which the excess solution was blown off with compressed air. AFM images were obtained by using a dynamic force microscope (Nanoscope-RIIIa; Digital Instruments, Santa Barbara, CA).

CD Spectroscopy. Aβ (1–40) monomer (50 μM) was dissolved in 50 mM sodium phosphate (pH 7.5) and 100 mM NaCl and incubated in the absence or presence of 5 μM L-PGDS/β-trace at 37°C for 2 h. These samples were diluted 2-fold in the buffer described above, and far-UV CD spectra were recorded at 37°C by using a Jasco-600 spectropolarimeter equipped with a thermostat-controlled cell holder (Jasco, Tokyo, Japan). A quartz cuvette with a 0.1-cm path length was used. The data were presented as the mean residue mass ellipticity for the Aβ peptide.

Analysis of Aβ Deposition *in Vivo*. Under pentobarbital (50 mg/kg, i.p.) anesthesia, biotin-labeled Aβ (1–42) (100 μM; AnaSpec, San Jose, CA) was infused at a rate of 0.66 μl/min for 60 min into the lateral ventricle (coordinates relative to bregma: anterior–posterior 0.0-mm, lateral 2.0-mm, and 2.3-mm depth) of 4-month-old male L-PGDS$^{-/-}$ mice (30, 31) and human L-PGDS-Tg mice (32). At 3 h after administration, the mice were killed. Cryosections (30 μm) of mouse brain were prepared, fixed in ethanol, and incubated with avidin–biotin–peroxidase complex (2 μg/ml; Vector Laboratories) according to the manufacturer's protocol. Cryosections were also stained with 1% Congo-red solution. For quantification of Aβ deposition, cryosections of mouse brain (30 μm) were fixed in ethanol and incubated with [^{125}I]-streptavidin (9.25 kBq/ml, 1,850 kBq/μg; Amersham Biosciences, Little Chalfont, U.K.) in 50 mM sodium phosphate (pH 7.5) and 100 mM NaCl for 2 h. After wash by 50 mM sodium phosphate (pH 7.5) and 100 mM NaCl containing 0.2% Triton X-100, the amount of biotin-labeled Aβ (1–42) within the brain was quantified with a Micro Imager radioisotope detector (Biospace Measures, Paris, France).

SI. Additional results about the inhibition of seed-dependent Aβ aggregation by L-PGDS/β-trace or human serum albumin can be found in SI Fig. 7.

We thank Dr. O. Hayaishi for his critical advice in this study, Dr. K. Yamaguchi for help with AFM measurements, and Dr. M. Mase for providing the human CSF samples.

1. Sisodia SS (1999) *J Clin Invest* 104:1169–1170.
2. Selkoe DJ (2001) *Physiol Rev* 81:741–766.
3. Hardy J, Selkoe DJ (2002) *Science* 297:353–356.
4. Tanzi RE, Kovacs DM, Kim TW, Moir RD, Guenette SY, Wasco W (1996) *Neurobiol Dis* 3:159–168.
5. Tanzi RE (1999) *J Clin Invest* 104:1175–1179.
6. Scubert P, Vigo-Pelfrey C, Esch F, Lee M, Dovey H, Davis D, Sinha S, Schlossmacher M, Whaley J, Swindlehurst C, *et al.* (1992) *Nature* 359:325–327.
7. Urade Y, Hayaishi O (2000) *Biochim Biophys Acta* 1482:259–271.
8. Urade Y, Eguch N, Hayaishi O (2006) in *Lipocalins*, ed Akerstrom B, Borregaard N, Flower D, Salier JP (Eurekah.com, Georgetown, TX), pp 99–109.
9. Clausen J (1961) *Proc Soc Exp Biol Med* 107:170–172.
10. Urade Y, Kitahama K, Ohishi H, Kaneko T, Mizuno N, Hayaishi O (1993) *Proc Natl Acad Sci USA* 90:9070–9074.
11. Beuckmann CT, Lazarus M, Gerashchenko D, Mizoguchi A, Nomura S, Mohri I, Uesugi A, Kaneko T, Mizuno N, Hayaishi O, Urade Y (2000) *J Comp Neurol* 428:62–78.
12. Hiraoka A, Arato T, Tominaga I, Anjyo A (1997) *J Pharm Biomed Anal* 15:1257–1263.
13. Einstein ER (1982) *Proteins of the Brain and CSF in Health and Disease* (Thomas, Springfield, IL).
14. Raman B, Ban T, Sakai M, Pasta SY, Ramakrishna T, Naiki H, Goto Y, Rao Ch M (2005) *Biochem J* 392:573–581.
15. Petkova AT, Ishii Y, Balbach JJ, Antzutkin ON, Leapman RD, Delaglio F, Tycko R (2002) *Proc Natl Acad Sci USA* 99:16742–16747.
16. Harper JD, Lansbury PT, Jr (1997) *Annu Rev Biochem* 66:385–407.
17. Wisniewski T, Frangione B (1992) *Neurosci Lett* 135:235–238.
18. Naslund J, Thyberg J, Tjernberg LO, Wernstedt C, Karlstrom AR, Bogdanovic N, Gandy SE, Lannfelt L, Terenius L, Nordstedt C, *et al.* (1995) *Neuron* 15:219–228.
19. Schwarzman AL, Gregori L, Vitek MP, Lyubski S, Strittmatter WJ, Enghilde JJ, Bhasin R, Silverman J, Weisgraber KH, Coyle PK, *et al.* (1994) *Proc Natl Acad Sci USA* 91:8368–8372.
20. Pitas RE, Boyles JK, Lee SH, Hui D, Weisgraber KH (1987) *J Biol Chem* 262:14352–14360.
21. Golabek AA, Soto C, Vogel T, Wisniewski T (1996) *J Biol Chem* 271:10602–10606.
22. Puchades M, Hansson SF, Nilsson CL, Andreasen N, Blennow K, Davidsson P (2003) *Brain Res Mol Brain Res* 118:140–146.
23. Shumaker SA, Legault C, Rapp SR, Thal L, Wallace RB, Ockene JK, Hendrix SL, Jones BN, III, Assaf AR, Jackson RD, *et al.* (2003) *J Am Med Assoc* 289:2651–2662.
24. Mong JA, Devidze N, Frail DE, O'Connor LT, Samuel M, Choleris E, Ogawa S, Pfaff DW (2003) *Proc Natl Acad Sci USA* 100:318–323.
25. Urade Y, Tanaka T, Eguchi N, Kikuchi M, Kimura H, Toh H, Hayaishi O (1995) *J Biol Chem* 270:1422–1428.
26. Beuckmann CT, Aoyagi M, Okazaki I, Hiroike T, Toh H, Hayaishi O, Urade Y (1999) *Biochemistry* 38:8006–8013.
27. Kimpara T, Takeda A, Yamaguchi T, Arai H, Okita N, Takase S, Sasaki H, Itoyama Y (2000) *Neurobiol Aging* 21:551–554.
28. Lazarov O, Robinson J, Tang YP, Hairston IS, Korade-Mirnics Z, Lee VM, Hersh LB, Sapolsky RM, Mirnics K, Sisodia SS (2005) *Cell* 120:701–713.
29. Hsiao K, Chapman P, Nilsen S, Eckman C, Harigaya Y, Younkin S, Yang F, Cole G (1996) *Science* 274:99–102.
30. Eguchi N, Minami T, Shirafuji N, Kanaoka Y, Tanaka T, Nagata A, Yoshida N, Urade Y, Ito S, Hayaishi O (1999) *Proc Natl Acad Sci USA* 96:726–730.
31. Qu WM, Huang ZL, Xu XH, Aritake K, Eguchi N, Nambu F, Narumiya S, Urade Y, Hayaishi O (2006) *Proc Natl Acad Sci USA* 103:17949–17954.
32. Pinzar E, Kanaoka Y, Inui T, Eguchi N, Urade Y, Hayaishi O (2000) *Proc Natl Acad Sci USA* 97:4903–4907.
33. Oda H, Shiina Y, Seiki K, Sato N, Eguchi N, Urade Y (2002) *Clin Chem* 48:1445–1453.
34. Oda H, Eguchi N, Urade Y, Hayaishi O (1996) *Proc Jpn Acad* 72:108–111.
35. Inui T, Ohkubo T, Emi M, Irikura D, Hayaishi O, Urade Y (2003) *J Biol Chem* 278:2845–2852.
36. Naiki H, Higuchi K, Hosokawa M, Takeda T (1989) *Anal Biochem* 177:244–249.
37. Ban T, Goto Y (2006) *Methods Enzymol* 413:91–102.
38. Fabien S, Annelies R, Laurent D (2004) Unexamined Patent FR2848573A1.

Acta Neuropathol (2007) 114:5–22
DOI 10.1007/s00401-007-0237-2

CONSENSUS PAPER

Neuropathologic diagnostic and nosologic criteria for frontotemporal lobar degeneration: consensus of the Consortium for Frontotemporal Lobar Degeneration

Nigel J. Cairns · Eileen H. Bigio · Ian R. A. Mackenzie · Manuela Neumann · Virginia M. -Y. Lee · Kimmo J. Hatanpaa · Charles L. White III · Julie A. Schneider · Lea Tenenholz Grinberg · Glenda Halliday · Charles Duyckaerts · James S. Lowe · Ida E. Holm · Markus Tolnay · Koichi Okamoto · Hideaki Yokoo · Shigeo Murayama · John Woulfe · David G. Munoz · Dennis W. Dickson · Paul G. Ince · John Q. Trojanowski · David M. A. Mann

Received: 9 May 2007 / Accepted: 9 May 2007 / Published online: 20 June 2007

Abstract The aim of this study was to improve the neuropathologic recognition and provide criteria for the pathological diagnosis in the neurodegenerative diseases grouped as frontotemporal lobar degeneration (FTLD); revised criteria are proposed. Recent advances in molecular genetics, biochemistry, and neuropathology of FTLD prompted the Midwest Consortium for Frontotemporal Lobar Degeneration and experts at other centers to review and revise the existing neuropathologic diagnostic criteria for FTLD. The proposed criteria for FTLD are based on existing criteria, which include the tauopathies [FTLD with Pick bodies, corticobasal degeneration, progressive supranuclear palsy, sporadic multiple system tauopathy with dementia, argyrophilic grain disease, neurofibrillary tangle dementia, and

N. J. Cairns
Department of Neurology,
Washington University School of Medicine,
Campus Box 8118, 660 South Euclid Avenue,
St Louis, MO 63110, USA

N. J. Cairns (✉)
Department of Pathology and Immunology,
Washington University School of Medicine,
Campus Box 8118, 660 South Euclid Avenue,
St Louis, MO 63110, USA
e-mail: cairns@wustl.edu

N. J. Cairns
Alzheimer's Disease Research Center,
Washington University School of Medicine,
Campus Box 8118, 660 South Euclid Avenue,
St Louis, MO 63110, USA

E. H. Bigio
Department of Pathology,
Northwestern University Feinberg School of Medicine,
Chicago, IL, USA

E. H. Bigio
Cognitive Neurology and Alzheimer Disease Center,
Northwestern University Feinberg School of Medicine,
Chicago, IL, USA

I. R. A. Mackenzie
Department of Pathology and Laboratory Medicine,
Vancouver General Hospital, Vancouver, BC, Canada

M. Neumann
Center for Neuropathology and Prion Research,
Ludwig-Maximilians University, Munich, Germany

V. M.-Y. Lee · J. Q. Trojanowski
Department of Pathology and Laboratory Medicine,
Center for Neurodegenerative Disease Research,
University of Pennsylvania School of Medicine,
Philadelphia, PA, USA

J. Q. Trojanowski
Institute on Aging,
University of Pennsylvania School of Medicine,
Philadelphia, PA, USA

K. J. Hatanpaa · C. L. White III
Neuropathology Laboratory, Department of Pathology,
University of Texas Southwestern Medical School,
Dallas, TX, USA

J. A. Schneider
Rush Alzheimer's Disease Center,
Rush University Medical School,
Chicago, IL, USA

L. T. Grinberg
Department of Pathology and Instituto Israelita
de Ensino e Pesquisa Albert Einstein, Faculdade
de Medicina, Universidade de São Paulo, Sao Paulo, Brazil